Figure 2. Associations of the *AFF1* locus with SLE. (A) A chromosomal plot of P-values in GWAS for SLE. (B) A regional plot in the *AFF1* locus. Diamond-shaped data points represent $-\log_{10}$ (P-values) of the SNPs. Large-sized points indicate the P-values of the landmark SNP, rs340630 (green for the combined study and red for the GWAS). Density of red color represents r^2 values with rs340630. Blue line represents recombination rates. Lower part indicates RefSeq genes. Gray dashed horizontal lines represent the threshold of $P = 5.0 \times 10^{-8}$. The plots were drawn using SNAP, version 2.1 [47].
doi:10.1371/journal.pgen.1002455.g002

Medical University, the University of Tokyo, and the BioBank Japan Project [36]. All subjects were of Japanese origin and provided written informed consent. SLE cases met the revised American College of Rheumatology (ACR) criteria for SLE [37]. Control subjects were confirmed to be free of autoimmune disease. Some of the SLE cases were included in our previous studies [38–40]. Details of the subjects are summarized in Table S1 and S2. This research project was approved by the ethical committees of the University of Tokyo, RIKEN, and affiliated medical institutes.

— 231 —

Table 2. Associations among previously reported SLE-related loci.

rsID	Chr	Position (bp)	Cytoband	Gene	Allele[a] 1/2	Allele 1 freq. Case	Allele 1 freq. Control	OR (95%CI)	P	eQTL[b]	Identified by the studies in[c] Caucasians	Identified by the studies in[c] Asians
rs2205960	1	171,458,098	1q25	TNFSF4	T/G	0.23	0.18	1.35 (1.19–1.54)	3.0×10^{-6}		+	
rs3024505	1	205,006,527	1q32	IL10	A/G	0.019	0.014	1.34 (0.90–2.00)	0.15		+	
rs13385731	2	33,555,394	2p22	RASGRP3	C/T	0.90	0.87	1.37 (1.15–1.64)	6.0×10^{-4}	+		+
rs10168266	2	191,644,049	2q32	STAT4	T/C	0.37	0.27	1.59 (1.42–1.78)	2.7×10^{-16}			+
rs6445975	3	58,345,217	3p14	PXK	G/T	0.25	0.23	1.09 (0.96–1.23)	0.18	+	+	
rs10516487	4	102,970,099	4q24	BANK1	G/A	0.91	0.89	1.28 (1.07–1.53)	0.0070			+
rs10036748	5	150,438,339	5q33	TNIP1	T/C	0.75	0.72	1.16 (1.03–1.31)	0.014			+
rs9501626	6	32,508,322	6p21	HLA-DRB1	A/C	0.20	0.12	1.86 (1.62–2.13)	1.0×10^{-18}			+
rs548234	6	106,674,727	6q21	PRDM1	C/T	0.40	0.34	1.30 (1.16–1.44)	2.3×10^{-6}	+	+	
rs2230926	6	138,237,759	6q23	TNFAIP3	G/T	0.11	0.069	1.75 (1.47–2.08)	1.9×10^{-10}	+	+	
rs849142	7	28,152,416	7p15	JAZF1	C/T	0.999	0.999	2.72 (0.25–29.8)	0.41		+	
rs4917014	7	50,276,409	7p12	IKZF1	T/G	0.58	0.53	1.24 (1.11–1.38)	8.1×10^{-5}			+
rs6964720	7	75,018,280	7q11	HIP1	G/A	0.25	0.19	1.43 (1.27–1.62)	1.3×10^{-8}			+
rs4728142	7	128,361,203	7q32	IRF5	A/G	0.16	0.11	1.48 (1.28–1.72)	2.4×10^{-7}	+	+	
rs2254546	8	11,381,089	8p23	BLK	G/A	0.78	0.72	1.42 (1.25–1.61)	4.1×10^{-8}	+	+	
rs1913517	10	49,789,060	10q11	WDFY4	A/G	0.32	0.28	1.20 (1.07–1.35)	0.0013			+
rs4963128	11	579,564	11p15	KIAA1542	T/C	0.98	0.97	1.58 (1.03–2.44)	0.038	+	+	
rs2732552	11	35,041,168	11p13	PDHX, CD44	T/C	0.75	0.73	1.13 (1.00–1.27)	0.056			+
rs4639966	11	118,078,729	11q23	Intergenic	T/C	0.32	0.28	1.22 (1.09–1.36)	7.3×10^{-4}			+
rs6590330	11	127,816,269	11q24	ETS1	A/G	0.48	0.39	1.44 (1.30–1.60)	1.3×10^{-11}			+
rs1385374	12	127,866,647	12q24	SLC15A4	T/C	0.19	0.16	1.21 (1.06–1.38)	0.0057			+
rs7329174	13	40,456,110	13q14	ELF1	G/A	0.30	0.25	1.32 (1.18–1.49)	2.2×10^{-6}			+
rs7197475	16	30,550,368	16p11	Intergenic	T/C	0.12	0.10	1.20 (1.02–0.41)	0.031			+
rs11150610	16	31,241,737	16p11	ITGAM	C/A	0.20	0.19	1.07 (0.94–1.22)	0.32	+	+	
rs12949531	17	13,674,531	17p12	Intergenic	T/C	0.28	0.27	1.02 (0.91–1.15)	0.73			+
rs463426	22	20,139,185	22q11	HIC2,UBE2L3	T/C	0.52	0.48	1.20 (1.08–1.33)	6.1×10^{-4}			+

[a]Based on forward strand of NCBI Build 36.3.
[b]Defined using gene expression data measured in lymphoblastoid B cell lines [28].
[c]Based on the previously reported studies for SLE susceptibility loci [3–18].
SLE, systemic lupus erythematosus; OR, odds ratio; eQTL, expression quantitative trait locus; GWAS, genome-wide association study.
doi:10.1371/journal.pgen.1002455.t002

Genotyping and quality control

In GWAS, 946 SLE cases and 3,477 controls were genotyped using Illumina HumanHap610-Quad and Illumina Human-Hap550v3 Genotyping BeadChips (Illumina, CA, USA), respectively. After the exclusion of 47 SLE cases and 92 controls with call rates <0.98, SNPs with call rates <0.99 in SLE cases or controls,

Table 3. Results of combined study for Japanese patients with SLE.

rsID	Chr	Position (bp)	Cytoband	Gene	Allele 1/2	Stage	No. subjects Case	No. subjects Control	Allele 1 freq. Case	Allele 1 freq. Control	OR (95%CI)	P	eQTL[a]
rs340630	4	88,177,419	4q21	AFF1	A/G	GWAS	891	3,383	0.56	0.51	1.22 (1.10–1.36)	1.5×10^{-4}	+
						Replication study 1	550	646	0.57	0.49	1.40 (1.19–1.64)	4.6×10^{-5}	
						Replication study 2	820	27,911	0.56	0.53	1.14 (1.03–1.26)	0.0094	
						Combined study	2,261	31,940	0.56	0.52	1.21 (1.14–1.30)	8.3×10^{-9}	

[a]Defined using gene expression data measured in lymphoblastoid B cell lines [28].
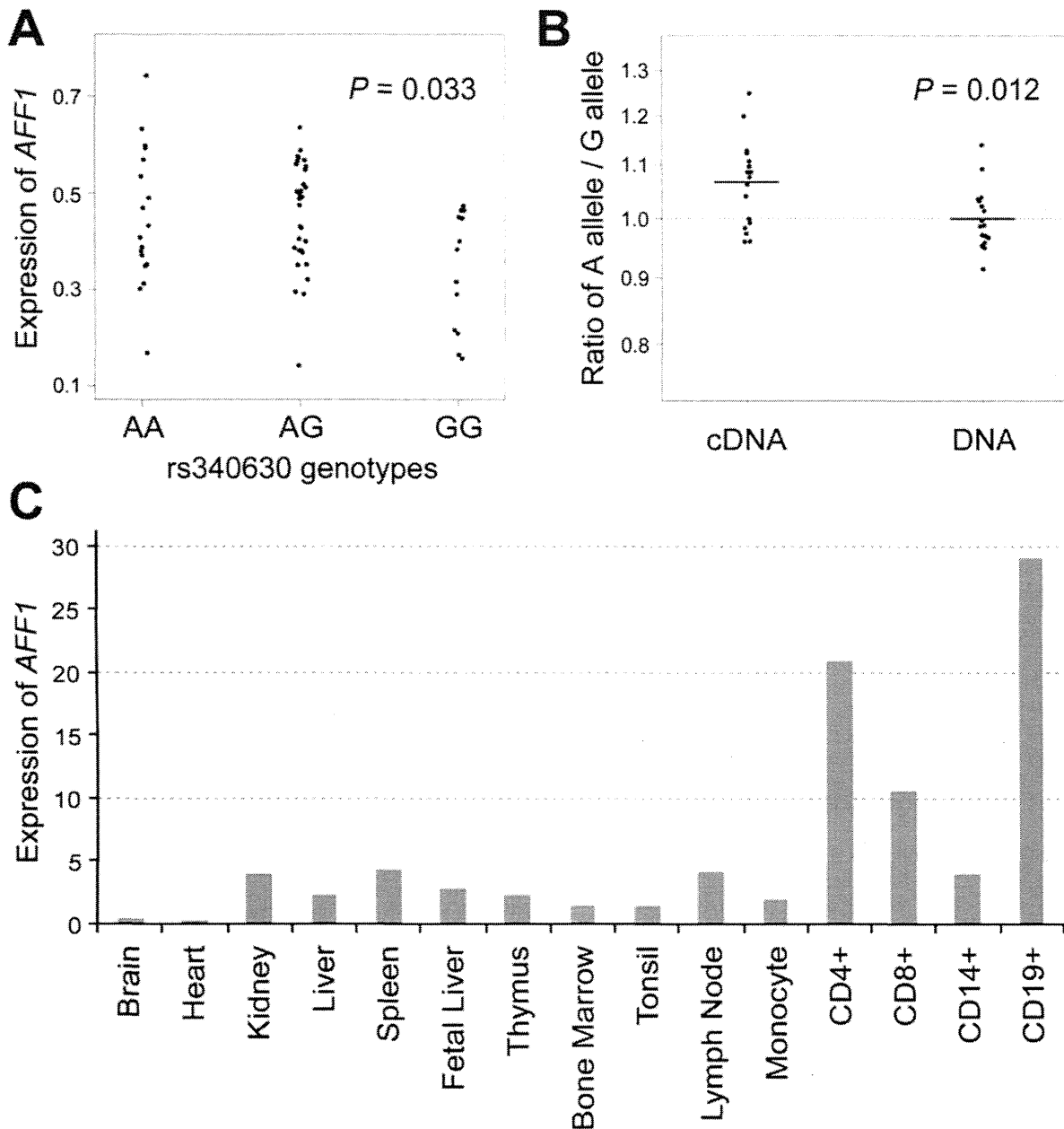doi:10.1371/journal.pgen.1002455.t003

— 232 —

Figure 3. Association of rs340630 with *AFF1* expression. (A) Correlation between rs340630 genotypes and transcript levels of *AFF1* (NM_001166693) in EBV-transfected cell lines ($n = 62$) stimulated with PMA. (B) Allele-specific quantification (ASTQ) of *AFF1* transcripts. Allele specific-probes for rs340638 were used for quantification by qPCR. The ratios of A allele over G allele for the amounts of both cDNAs and DNAs were plotted in log scale for each cell line. (C) *AFF1* expression in various tissues. Transcripts levels of *AFF1* were quantified by qPCR and were normalized by *GAPDH* levels.
doi:10.1371/journal.pgen.1002455.g003

non-autosomal SNPs, and SNPs not shared between SLE cases and controls, were excluded. We excluded 7 closely related SLE cases in a 1st or 2nd degree of kinship based on identity-by-descent estimated using PLINK version 1.06 [41]. We then excluded 1 SLE cases and 1 controls whose ancestries were estimated to be distinct from East-Asian populations using PCA performed along with the genotype data of Phase II HapMap populations (release 24) [29] using EIGENSTRAT version 2.0 [42]. Subsequently,

SNPs with minor allele frequencies <0.01 in SLE cases or controls, SNPs with exact P-values of Hardy-Weinberg equilibrium test $<1.0 \times 10^{-6}$ in controls, or SNPs with ambiguous cluster plots were excluded. Finally, 430,797 SNPs for 891 SLE cases and 3,384 controls were obtained. Genotyping of SNPs in replication studies was performed using TaqMan Assay or Illumina HumanHap610-Quad Genotyping BeadChip (Illumina, CA, USA).

— 233 —

Association analysis of the SNPs

Association of SNPs in GWAS and replication studies were tested with Cochran-Armitage's trend test. Combined analysis was performed with Mantel-Haenzel method. Associations of previously reported SLE susceptibility loci [3–18] were evaluated using the results of the GWAS. Genotype imputation was performed for non-genotyped SNPs using MACH version 1.0 [43] with Phase II HapMap East-Asian individuals as references [29], as previously described [44]. All imputed SNPs demonstrated imputation scores, Rsq, >0.70.

eQTL study

We analyzed gene expression data previously measured in lymphoblastoid B cell lines from Phase II HapMap East-Asian individuals using Illumina's human whole-genome expression array (WG-6 version 1) (accession number; GSE6536) [28]. Expression data were normalized across the individuals. We used BLAST to map 47,294 Illumina array probes onto human autosomal reference genome sequences (Build 36). We discarded probes mapped with expectation values smaller than 0.01 to multiple loci, or for which there was polymorphic HapMap SNP(s) inside the probe. Then, 19,047 probes with exact matches to a unique locus with 100% identity and with a mean signal intensity greater than background were obtained. Genotype data of HapMap individuals were obtained for SNPs included in the GWAS. Associations of SNP genotypes (coded as 0, 1, and 2) with expression levels of each of the cis-eQTL probes (located within ±300 kbp regions of the SNPs) were evaluated using linear regression assuming additive effects of the genotypes on the expression levels. Considering the significant overlap between eQTL and genetic loci responsible for autoimmune diseases [24], we applied relatively less stringent multiple testing threshold of FDR Q-values<0.2 for the definition of eQTL. SNPs that exhibited this threshold with any of the corresponding cis-eQTL probes were denoted as eQTL positive.

Selection of SNPs enrolled in the replication studies

In order to select SNPs for further replication studies, we firstly integrated the results of GWAS and eQTL study. SNPs that satisfied $P<1.0\times10^{-4}$ in GWAS, or the SNPs that satisfied $1.0\times10^{-4}\leq P<1.0\times10^{-3}$ in GWAS and denoted as eQTL positive, were selected. Among these, SNPs most significantly associated in each of the genomic loci and not included in the previously reported SLE susceptibility loci [3–18] were further evaluated.

Then, the results of the concurrently proceeding genome-wide scan for SLE in the Japanese subjects using a pooled DNA approach were referred (Tahira T et al. Presented at the 59th Annual Meeting of the American Society of Human Genetics, October 21, 2009). In the scan, DNA collected from 447 SLE cases and 680 controls of Japanese origin were pooled respectively, and genotyped using GeneChip Human Mapping 500K Array Set (Affymetrix, CA, USA). SNPs were ranked according to the Silhouette scores estimated based on relative allele scores (RAS) between SLE cases and controls, and rank-based P-values were assigned [30]. By referring to association signals in multiple neighboring SNPs in the pooled analysis, we selected SNPs for replication study 1. Namely, if the SNP of interest was in LD ($r^2>0.5$) or was located within ±100 kbp of SNPs showing association signals in the pooled analysis (rank-based $P<0.01$), it would be selected. SNPs that satisfied $P<1.0\times10^{-6}$ in the combined study of GWAS and replication study 1 were further evaluated in replication study 2 (Figure 1).

Quantification of *AFF1* expression

EBV-transformed lymphoblastoid cell lines ($n=62$) were established by Pharma SNP Consortium (Tokyo, Japan) using peripheral blood lymphocytes of Japanese healthy individuals. Cells were incubated for 2 h in medium alone (RPMI 1640 medium containing 10% FBS, 1% penicillin, and 1% streptomycin) or with 100 ng/ml PMA. Conditions for cell stimulation were optimized before the experiment as previously described [45]. Cells were then harvested and total RNA was isolated using an RNeasy Mini Kit (Qiagen) with DNase treatment. Total RNA (1 µg) was reverse transcribed using TaqMan Gold RT-PCR reagents with random hexamers (Applied Biosystems). Real-time quantitative PCR was performed in triplicate using an ABI PRISM 7900 and TaqMan gene expression assays (Applied Biosystems). Specific probes (Hs01089428_m1) for transcript of *AFF1* (NM_001166693) were used. Expression of *AFF1* in various tissues was also quantified using Premium Total RNA (Clontech). The data were normalized to *GAPDH* levels. *GUS* levels were also evaluated for internal control, and similar results were obtained. Correlation coefficient, R^2, between rs340630 genotypes and transcript levels of *AFF1* was evaluated.

Allele-specific transcript quantification (ASTQ)

ASTQ of *AFF1* in PSC cells was performed as previously described [46]. DNAs were extracted by using a DNeasy Kit (QIAGEN). RNA extraction and cDNA preparation were performed as described above. For PSC cells ($n=17$) that were heterozygous for both rs340630 (the landmark SNP of GWAS) and rs340638 (located in the 5'-untranslated region of *AFF1* and in absolute LD with rs340630), expression levels of *AFF1* were quantified by qPCR on an ABI Prism 7900 using a custom-made TaqMan MGB-probe set for rs340638. Primer sequences were 5'-CTAACTGTGGCCCGCGTTG-3' and 5'-CCCGGCGCA-GTTTCTGAG-3'. The probe sequences were 5'-VIC-CGAA-GACCGCCAGCGCCCAAC-TAMRA-3' and 5'-FAM-CGAA-GACCGCCGGCGCCCAA-TAMRA-3'. Ct values of VIC and FAM were obtained for genomic DNA and cDNA samples after 40 cycles of real-time PCR. We also prepared genomic DNA of samples homozygous for each allele and mixed them at different ratios (2:8, 3:7, 4:6, 5:5, 6:4, 7:3, 8:2) to create a standard curve by plotting Ct values of VIC/FAM against the allelic ratio of VIC/FAM for each mixture. Using the standard curve, we calculated the allelic ratios for each genomic DNA and cDNA samples. We measured each sample in quadruplicate in one assay; tests were independently repeated twice.

Web resources

The URLs for data presented herein are as follows.

NCBI GEO, http://www.ncbi.nlm.nih.gov/geo

BioBank Japan Project, http://biobankjp.org

PLINK software, http://pngu.mgh.harvard.edu/~purcell/plink/index.shtml

International HapMap Project, http://www.hapmap.org

EIGENSTRAT software, http://genepath.med.harvard.edu/~reich/Software.htm

MACH and mach2qtl software, http://www.sph.umich.edu/csg/abecasis/MACH/index.html

SNAP, http://www.broadinstitute.org/mpg/snap/index.php

Supporting Information

Figure S1 Principal component analysis (PCA) plot of the subjects. PCA plot of subjects enrolled in the GWAS for SLE. SLE cases and the controls enrolled in the GWAS are plotted based on

eigenvectors 1 and 2 obtained from the PCA using EIGEN-STRAT version 2.0 [42], along with European (CEU), African (YRI), Japanese (JPT), and Chinese (CHB) individuals obtained from the Phase II HapMap database (release 22) [29]. Subjects who were estimated to be outliers in terms of ancestry from East-Asian (JPT+CHB) clusters and excluded from the study are indicated by black arrows.
(TIF)

Figure S2 Quantile-Quantile plot (QQ-plot) of *P*-values in the GWAS for SLE. The horizontal axis indicates the expected $-\log_{10}$ (*P*-values). The vertical axis indicates the observed $-\log_{10}$ (*P*-values). The QQ-plot for the *P*-values of all SNPs that passed the quality control criteria is indicated in blue. The QQ-plot for the *P*-values after the removal of SNPs included in the previously reported SLE susceptibility loci is indicated in black. The gray line represents $y = x$. The SNPs for which the *P*-value was smaller than 1.0×10^{-15} are indicated at the upper limit of the plot.
(TIF)

Table S1 Basal characteristics of cohorts.
(DOC)

Table S2 Frequency of clinical characteristics of SLE in this GWAS.
(DOC)

Table S3 Distributions of eQTL positivity rates of the SNPs.
(DOC)

Table S4 Results of replication study 1 for Japanese patients with SLE.
(DOC)

Table S5 Results of replication studies 1 and 2 for Japanese patients with SLE.
(DOC)

Acknowledgments

Author Contributions

Conceived and designed the experiments: Y. Okada, K. Shimane, Y. Kochi, A. Suzuki, M. Kubo, N. Kamatani, R. Yamada, Y. Nakamura, K. Yamamoto. Performed the experiments: Y. Kochi, N. Hosono, M. Kubo, K. Myouzen, T. Horiuchi, T. Tahira, K. Hayashi. Analyzed the data: Y. Okada, A. Takahashi, T. Tsunoda, K. Higasa, R. Yamada. Contributed reagents/materials/analysis tools: T. Horita, T. Atsumi, T. Koike, T. Ishii, A. Okamoto, K. Fujio, M. Hirakata, H. Amano, Y. Takasaki, Y. Kondo, S. Ito, T. Sumida, K. Takada, A. Mimori, K. Saito, Y. Tanaka, M. Kamachi, N. Nishimoto, Y. Kawaguchi, C. Terao, K. Ohmura, T. Mimori, F. Matsuda, O.W. Mohammed, K. Matsuda, K. Shimane, K. Ikari, H. Yamanaka. Wrote the paper: Y. Okada, K. Shimane, Y. Kochi, A. Suzuki, R. Yamada, K. Yamamoto.

References

1. Lipsky PE (2001) Systemic lupus erythematosus: an autoimmune disease of B cell hyperactivity. Nat Immunol 2: 764–766.
2. Sestak AL, Shaver TS, Moser KL, Neas BR, Harley JB (1999) Familial aggregation of lupus and autoimmunity in an unusual multiplex pedigree. J Rheumatol 26: 1495–1499.
3. Sigurdsson S, Nordmark G, Goring HH, Lindroos K, Wiman AC, et al. (2005) Polymorphisms in the tyrosine kinase 2 and interferon regulatory factor 5 genes are associated with systemic lupus erythematosus. Am J Hum Genet 76: 528–537.
4. Graham RR, Kozyrev SV, Baechler EC, Reddy MV, Plenge RM, et al. (2006) A common haplotype of interferon regulatory factor 5 (IRF5) regulates splicing and expression and is associated with increased risk of systemic lupus erythematosus. Nat Genet 38: 550–555.
5. Graham RR, Kyogoku C, Sigurdsson S, Vlasova IA, Davies LR, et al. (2007) Three functional variants of IFN regulatory factor 5 (IRF5) define risk and protective haplotypes for human lupus. Proc Natl Acad Sci U S A 104: 6758–6763.
6. Remmers EF, Plenge RM, Lee AT, Graham RR, Hom G, et al. (2007) STAT4 and the risk of rheumatoid arthritis and systemic lupus erythematosus. N Engl J Med 357: 977–986.
7. Cunninghame Graham DS, Graham RR, Manku H, Wong AK, Whittaker JC, et al. (2008) Polymorphism at the TNF superfamily gene TNFSF4 confers susceptibility to systemic lupus erythematosus. Nat Genet 40: 83–89.
8. Nath SK, Han S, Kim-Howard X, Kelly JA, Viswanathan P, et al. (2008) A nonsynonymous functional variant in integrin-alpha(M) (encoded by ITGAM) is associated with systemic lupus erythematosus. Nat Genet 40: 152–154.
9. Harley JB, Alarcon-Riquelme ME, Criswell LA, Jacob CO, Kimberly RP, et al. (2008) Genome-wide association scan in women with systemic lupus erythematosus identifies susceptibility variants in ITGAM, PXK, KIAA1542 and other loci. Nat Genet 40: 204–210.
10. Kozyrev SV, Abelson AK, Wojcik J, Zaghlool A, Linga Reddy MV, et al. (2008) Functional variants in the B-cell gene BANK1 are associated with systemic lupus erythematosus. Nat Genet 40: 211–216.
11. Hom G, Graham RR, Modrek B, Taylor KE, Ortmann W, et al. (2008) Association of systemic lupus erythematosus with C8orf13-BLK and ITGAM-ITGAX. N Engl J Med 358: 900–909.
12. Graham RR, Cotsapas C, Davies L, Hackett R, Lessard CJ, et al. (2008) Genetic variants near TNFAIP3 on 6q23 are associated with systemic lupus erythematosus. Nat Genet 40: 1059–1061.
13. Musone SL, Taylor KE, Lu TT, Nititham J, Ferreira RC, et al. (2008) Multiple polymorphisms in the TNFAIP3 region are independently associated with systemic lupus erythematosus. Nat Genet 40: 1062–1064.
14. Han JW, Zheng HF, Cui Y, Sun LD, Ye DQ, et al. (2009) Genome-wide association study in a Chinese Han population identifies nine new susceptibility loci for systemic lupus erythematosus. Nat Genet 41: 1234–1237.
15. Gateva V, Sandling JK, Hom G, Taylor KE, Chung SA, et al. (2009) A large-scale replication study identifies TNIP1, PRDM1, JAZF1, UHRF1BP1 and IL10 as risk loci for systemic lupus erythematosus. Nat Genet 41: 1228–1233.
16. Yang W, Shen N, Ye DQ, Liu Q, Zhang Y, et al. (2010) Genome-wide association study in Asian populations identifies variants in ETS1 and WDFY4 associated with systemic lupus erythematosus. PLoS Genet 6: e1000841. doi:10.1371/journal.pgen.1000841.
17. Lessard CJ, Adrianto I, Kelly JA, Kaufman KM, Grundahl KM, et al. (2011) Identification of a systemic lupus erythematosus susceptibility locus at 11p13 between PDHX and CD44 in a multiethnic study. Am J Hum Genet 88: 83–91.
18. Yang J, Yang W, Hirankarn N, Ye DQ, Zhang Y, et al. (2011) ELF1 is associated with systemic lupus erythematosus in Asian populations. Hum Mol Genet 20: 601–607.
19. Hopkinson ND, Doherty M, Powell RJ (1994) Clinical features and race-specific incidence/prevalence rates of systemic lupus erythematosus in a geographically complete cohort of patients. Ann Rheum Dis 53: 675–680.
20. Danchenko N, Satia JA, Anthony MS (2006) Epidemiology of systemic lupus erythematosus: a comparison of worldwide disease burden. Lupus 15: 308–318.
21. Yang J, Benyamin B, McEvoy BP, Gordon S, Henders AK, et al. (2010) Common SNPs explain a large proportion of the heritability for human height. Nat Genet 42: 565–569.
22. Raychaudhuri S, Plenge RM, Rossin EJ, Ng AC, Purcell SM, et al. (2009) Identifying relationships among genomic disease regions: predicting genes at pathogenic SNP associations and rare deletions. PLoS Genet 5: e1000534. doi:10.1371/journal.pgen.1000534.
23. Cantor RM, Lange K, Sinsheimer JS (2010) Prioritizing GWAS results: A review of statistical methods and recommendations for their application. Am J Hum Genet 86: 6–22.
24. Dubois PC, Trynka G, Franke L, Hunt KA, Romanos J, et al. (2010) Multiple common variants for celiac disease influencing immune gene expression. Nat Genet 42: 295–302.
25. Cookson W, Liang L, Abecasis G, Moffatt M, Lathrop M (2009) Mapping complex disease traits with global gene expression. Nat Rev Genet 10: 184–194.
26. Kochi Y, Okada Y, Suzuki A, Ikari K, Terao C, et al. (2010) A regulatory variant in CCR6 is associated with rheumatoid arthritis susceptibility. Nat Genet 42: 515–519.
27. Yamaguchi-Kabata Y, Nakazono K, Takahashi A, Saito S, Hosono N, et al. (2008) Japanese population structure, based on SNP genotypes from 7003 individuals compared to other ethnic groups: effects on population-based association studies. Am J Hum Genet 83: 445–456.
28. Stranger BE, Nica AC, Forrest MS, Dimas A, Bird CP, et al. (2007) Population genomics of human gene expression. Nat Genet 39: 1217–1224.
29. The International HapMap Consortium (2003) The International HapMap Project. Nature 426: 789–796.

— 235 —

30. Pearson JV, Huentelman MJ, Halperin RF, Tembe WD, Melquist S, et al. (2007) Identification of the genetic basis for complex disorders by use of pooling-based genomewide single-nucleotide-polymorphism association studies. Am J Hum Genet 80: 126–139.

31. Xia ZB, Popovic R, Chen J, Theisler C, Stuart T, et al. (2005) The MLL fusion gene, MLL-AF4, regulates cyclin-dependent kinase inhibitor CDKN1B (p27kip1) expression. Proc Natl Acad Sci U S A 102: 14028–14033.

32. Isnard P, Core N, Naquet P, Djabali M (2000) Altered lymphoid development in mice deficient for the mAF4 proto-oncogene. Blood 96: 705–710.

33. Schadt EE, Molony C, Chudin E, Hao K, Yang X, et al. (2008) Mapping the genetic architecture of gene expression in human liver. PLoS Biol 6: e107. doi:10.1371/journal.pbio.0060107.

34. Ernst J, Kheradpour P, Mikkelsen TS, Shoresh N, Ward LD, et al. (2011) Mapping and analysis of chromatin state dynamics in nine human cell types. Nature 473: 43–49.

35. Stahl EA, Raychaudhuri S, Remmers EF, Xie G, Eyre S, et al. (2010) Genome-wide association study meta-analysis identifies seven new rheumatoid arthritis risk loci. Nat Genet 42: 508–514.

36. Nakamura Y (2007) The BioBank Japan Project. Clin Adv Hematol Oncol 5: 696–697.

37. Hochberg MC (1997) Updating the American College of Rheumatology revised criteria for the classification of systemic lupus erythematosus. Arthritis Rheum 40: 1725.

38. Suzuki A, Yamada R, Kochi Y, Sawada T, Okada Y, et al. (2008) Functional SNPs in CD244 increase the risk of rheumatoid arthritis in a Japanese population. Nat Genet 40: 1224–1229.

39. Shimane K, Kochi Y, Horita T, Ikari K, Amano H, et al. (2010) The association of a nonsynonymous single-nucleotide polymorphism in TNFAIP3 with systemic lupus erythematosus and rheumatoid arthritis in the Japanese population. Arthritis Rheum 62: 574–579.

40. Myouzen K, Kochi Y, Shimane K, Fujio K, Okamura T, et al. (2010) Regulatory polymorphisms in EGR2 are associated with susceptibility to systemic lupus erythematosus. Hum Mol Genet 19: 2313–2320.

41. Purcell S, Neale B, Todd-Brown K, Thomas L, Ferreira MA, et al. (2007) PLINK: a tool set for whole-genome association and population-based linkage analyses. Am J Hum Genet 81: 559–575.

42. Price AL, Patterson NJ, Plenge RM, Weinblatt ME, Shadick NA, et al. (2006) Principal components analysis corrects for stratification in genome-wide association studies. Nat Genet 38: 904–909.

43. Li Y, Willer C, Sanna S, Abecasis G (2009) Genotype imputation. Annu Rev Genomics Hum Genet 10: 387–406.

44. Okada Y, Takahashi A, Ohmiya H, Kumasaka N, Kamatani Y, et al. (2011) Genome-wide association study for C-reactive protein levels identified pleiotropic associations in the IL6 locus. Hum Mol Genet 20: 1224–1231.

45. Aikawa Y, Yamamoto M, Yamamoto T, Morimoto K, Tanaka K (2002) An anti-rheumatic agent T-614 inhibits NF-kappaB activation in LPS- and TNF-alpha-stimulated THP-1 cells without interfering with IkappaBalpha degradation. Inflamm Res 51: 188–194.

46. Akamatsu S, Takata R, Ashikawa K, Hosono N, Kamatani N, et al. (2010) A functional variant in NKX3.1 associated with prostate cancer susceptibility down-regulates NKX3.1 expression. Hum Mol Genet 19: 4265–4272.

47. Johnson AD, Handsaker RE, Pulit SL, Nizzari MM, O'Donnell CJ, et al. (2008) SNAP: a web-based tool for identification and annotation of proxy SNPs using HapMap. Bioinformatics 24: 2938–2939.

— 236 —

The Pattern-Recognition Receptor Nucleotide-Binding Oligomerization Domain–Containing Protein 1 Promotes Production of Inflammatory Mediators in Rheumatoid Arthritis Synovial Fibroblasts

Kazuhiro Yokota,[1] Takashi Miyazaki,[2] Hossein Hemmatazad,[1] Renate E. Gay,[1] Christoph Kolling,[3] Ursula Fearon,[4] Hiromichi Suzuki,[2] Toshihide Mimura,[2] Steffen Gay,[1] and Caroline Ospelt[1]

Objective. Pattern-recognition receptors (PRRs), such as Toll-like receptors (TLRs) and nucleotide-binding oligomerization domain–containing protein 2 (NOD-2), have been shown to contribute to the pathogenesis of rheumatoid arthritis (RA). The aim of this study was to analyze the expression, regulation, and function of the PRR NOD-1 in RA synovial fibroblasts (RASFs), and to examine its interaction with other PRRs.

Methods. Expression of NOD-1 was analyzed by immunohistochemistry in synovial tissue from RA patients, psoriatic arthritis patients, gout patients, and osteoarthritis (OA) patients. RASFs and human monocyte-derived macrophages (HMDMs) were stimulated with L-alanyl-γ-D-glutamyl-meso-diaminopimelic acid, palmitoyl-3-cysteine-serine-lysine-4, poly(I-C), lipo-polysaccharide, heat-inactivated bacteria, tumor necrosis factor α (TNFα), or interleukin-1β (IL-1β). Expression levels of IL-6, CCL5, matrix metalloproteinases (MMPs), NODs, and TLRs were measured by real-time reverse transcription–polymerase chain reaction and/or enzyme-linked immunosorbent assay. NOD-1 and NOD-2 were silenced with target-specific small interfering RNA. Phosphorylation of IL-1 receptor–associated kinase 1 (IRAK-1) was measured by Western blotting.

Results. Expression of NOD-1 protein was significantly increased in RA synovium compared to OA synovium. The basal expression of NOD-1 was similar in RASFs, OASFs, healthy control peripheral blood mononuclear cells, and healthy control HMDMs. Stimulation of RASFs with TLR-3 up-regulated the expression of NOD-1. Expression of IL-6, CCL5, MMPs, TLR-2, and NOD-2 was significantly up-regulated in RASFs by stimulation with the NOD-1 ligand. A synergistic effect on IL-6 production was observed in cells stimulated with NOD-1 and TLR-2 ligands or NOD-1 and TLR-4 ligands. Silencing of NOD-1, but not NOD-2, decreased the levels of IL-6 in RASFs after stimulation with TLR-2 and IL-1β, and blocked the phosphorylation of IRAK-1.

Conclusion. NOD-1 is strongly expressed in different cell types in the synovial tissue of patients with RA. These results indicate that NOD-1, either alone or interacting with other inflammatory mediators, can play an important role in the chronic and destructive inflammation of the joints in RA.

Although the pathogenesis of rheumatoid arthritis (RA) remains as yet unclear, it has long been

1329

suggested that activation of the innate immune system by endogenous or exogenous stimuli plays a role (1,2). Fungal, bacterial, and viral pathogens, as well as endogenous danger signals (e.g., heat-shock proteins), are recognized by specific pattern-recognition receptors (PRRs), such as Toll-like receptors (TLRs) and nucleotide-binding oligomerization domain (NOD)–like receptors (NLRs). TLRs are cell-surface or endosomal receptors, whereas NLRs are cytosolic molecules. Both TLRs and NLRs mediate the production of proinflammatory mediators via the initiation of the transcription factor NF-κB and the MAP kinase cascade (3,4).

In previous studies, our group demonstrated that RA synovial fibroblasts (RASFs) express specific TLRs and the NLR NOD-2, and that activation of these PRRs plays a role in the pathogenesis of RA through the induction of proinflammatory cytokines, chemokines, and matrix-degrading enzymes (5–7). Together with NOD-2, NOD-1 belongs to the group of caspase activation and recruitment domain–containing NLRs and is known to be expressed in antigen-presenting cells and epithelial cells (8,9). NOD-1 can sense the peptidoglycan-related molecule diaminopimelic acid (DAP), which is a constituent of most gram-negative bacteria and specific gram-positive bacteria such as Listeria and Bacillus species (10).

NOD-1 has been found to be crucial for host defense against a variety of bacteria, including Helicobacter pylori and Chlamydiae (11,12). Accordingly, NOD-1 was shown to induce an inflammatory response in many different cell types and to synergize with TLRs to coordinate the immune defense (9,13,14). Moreover, a polymorphism in NOD-1 was shown to be associated with susceptibility to chronic inflammatory diseases such as asthma and inflammatory bowel disease (15,16).

To clarify the role of NOD-1 in RA and its possible interaction with other innate immune pathways, we analyzed its expression in RA synovial tissue and RASFs, and we characterized its patterns of expression, regulation, and function in synovial cells. The results reveal a novel role of NOD-1 in promoting TLR-2 signaling pathways in synovial fibroblasts.

PATIENTS AND METHODS

Collection of synovial tissue and culture of synovial fibroblasts, peripheral blood mononuclear cells (PBMCs), and human monocyte-derived macrophages (HMDMs). Samples of RA synovial tissue and osteoarthritis (OA) synovial tissue were obtained from patients undergoing joint replacement surgery at the Schulthess Clinic. In addition, synovial biopsy tissue was obtained from patients with gout or psoriatic arthritis (PsA). All patients signed a consent form prior to sample collection, and permission for the study was provided

by the local ethics authorities. Patients with RA fulfilled the American College of Rheumatology revised criteria for the classification of RA (17).

Synovial fibroblasts were isolated by digestion of the synovial tissue (150 mg/ml Dispase, at 37°C for 60 minutes), and then cultured in Dulbecco's minimum essential medium (Gibco Invitrogen) supplemented with 10% fetal calf serum (FCS), 50 units/ml penicillin/streptomycin, 2 mM L-glutamine, 10 mM HEPES, and 0.2% amphotericin B (all from Gibco Invitrogen). Cell cultures were maintained at 37°C in a humidified incubator (atmosphere of 5% CO_2). For these experiments, cultured synovial fibroblasts from passages 4–8 were used.

PBMCs were isolated from the blood of healthy donors using Ficoll-Paque Plus gradient centrifugation. For the generation of HMDMs, peripheral blood monocytes were isolated from the healthy control PBMCs with CD14 MACS Micro-Beads (Miltenyi Biotec), and 15 ng/ml macrophage colony-stimulating factor (HumanZyme) was added every 48 hours for 7 days. HMDMs and PBMCs were cultured in RPMI 1640 (Gibco Invitrogen) supplemented with 10% FCS, 50 units/ml penicillin/streptomycin, 2 mM L-glutamine, 10 mM HEPES, and 0.2% fungicide.

Immunohistochemical analysis. For immunohistochemical analyses, sections from formalin-fixed, paraffin-embedded synovial tissue were deparaffinized and pretreated at 80°C for 30 minutes in 10 mM citrate buffer (pH 6.0) for antigen retrieval. After washing in H_2O, sections were incubated with 3% H_2O_2. Washing in phosphate buffered saline (PBS)/0.05% Tween was followed by 1 hour of incubation in PBS/0.05% Tween/5% goat serum/1% bovine serum albumin (blocking buffer). The sections were incubated overnight at 4°C with rabbit anti-human NOD-1 antiserum (2 μg/ml; Alpha Diagnostic). As a negative control, rabbit IgG was used instead of the primary antibody. To show the binding specificity of the NOD-1 antibody, additional antibody-blocking experiments were performed, in which 1 μg antibody was incubated with or without 50 μg blocking peptide (Alpha Diagnostic) at 37°C for 2 hours, and then at 4°C for 24 hours. The solutions were centrifuged for 15 minutes at 14,000 revolutions per minute.

After washing, all slides were incubated for 30 minutes with horseradish peroxidase (HRP)–conjugated goat anti-rabbit IgG (Jackson ImmunoResearch). Antigen–antibody complexes were detected with aminoethylcarbazole chromogen substrate (DakoCytomation) and counterstained with hematoxylin. The intensity of the staining was evaluated in the lining and sublining layers of the synovial tissue by 2 observers (KY and CO), using a gradual scoring scale, ranging from 0 (no staining) to 4 (strong staining).

For immunofluorescence double stainings, deparaffinized slides were pretreated with 10 mM citrate buffer, as described above, followed by incubation in 1 mg/ml trypsin (Sigma-Aldrich) at 37°C for 20 minutes. Nonspecific protein binding was blocked with blocking buffer for 1 hour. Slides were incubated with rabbit anti-human NOD-1 antiserum along with mouse anti-human CD68 (clone PG-MA; DakoCytomation) or mouse anti-human vimentin (DakoCytomation) at 4°C for 24 hours (all at 2 μg/ml). Rabbit IgG and mouse IgG (each 2 μg/ml) served as negative controls. Goat anti-rabbit Texas Red–labeled antibodies and goat anti-mouse Alexa Fluor 488–labeled antibodies (both from Jackson Immuno-

Research) were used as secondary antibodies. Nuclei were stained with DAPI.

Stimulation experiments. Cells were stimulated with the following agents: 10 ng/ml L-alanyl-γ-D-glutamyl-meso-diaminopimelic acid (Tri-DAP; InvivoGen), 10 μg/ml poly(I-C) (PIC; InvivoGen), 100 ng/ml lipopolysaccharide (LPS) from *Esherichia coli* (List Biological Laboratories), 300 ng/ml palmitoyl-3-cysteine-serine-lysine-4 (Pam$_3$CSK$_4$; Invivo-Gen), 1 ng/ml interleukin-1β (IL-1β; R&D Systems), 10 ng/ml tumor necrosis factor α (TNFα; R&D Systems), 10^9 cells/ml heat-inactivated *Staphylococcus aureus* or heat-inactivated *Listeria monocytogenes* (InvivoGen), or 5 ng/ml polymyxin B (Sigma-Aldrich).

Quantitative real-time reverse transcription–polymerase chain reaction (RT-PCR). Total RNA was isolated using an RNeasy Mini kit (Qiagen), and complementary DNA was generated by RT using random hexamers and MultiScribe reverse transcriptase (Applied Biosystems). Messenger RNA (mRNA) expression levels were determined by TaqMan/SYBR Green real-time PCR on an ABI Prism 7500 sequence detection system (Applied Biosystems). The sequences of the primers and probes used for the detection of matrix metalloproteinases (MMPs) and TLRs have been previously described (6,7). The sequences of the SYBR primers were as follows: for NOD-1, forward GAG-CAA-AGT-CGT-GGT-CAA-CA and reverse GCT-GCT-GGG-TAT-ACC-TGC-TC; for NOD-2, forward TTC-TCC-GGG-TTG-TGA-AAT-GT and reverse CTC-CTC-TGT-GCC-TGA-AAA-GC; for IL-6, forward CTC-TTC-AGA-ACG-AAT-TGA-CAA-ACA-A and reverse GAG-ATG-CCG-TCG-ACG-ATG-TAC; and for CCL5, forward CTC-CCC-ATA-TTC-CTC-GGA-CA and reverse GCG-GGC-AAT-GTA-GGC-AAA. The expression of the housekeeping gene 18S was used as an endogenous control. For calculations of fold changes, the comparative threshold cycle method was used, as previously described (6).

Silencing of NOD-1. RASFs were transfected using an Amaxa Basic Nucleofector kit (Lonza) according to the manufacturer's protocol. Briefly, cells (5 × 10^5) were resuspended in 100 μl of transfection solution, with 2.0 μg of scrambled control small interfering RNA (siRNA) or NOD-1 siRNA (Ambion), and transfection was done using a Nucleofector device (Program U23). After 24 hours of transfection, the medium was changed and the cells were stimulated. Silencing of NOD-2 in the cells was done as previously described (7).

Enzyme-linked immunosorbent assays (ELISAs). The detection of IL-6 protein in cell supernatants was performed with an OptEIA kit (BD PharMingen) according to the manufacturer's instructions. For measurements of CCL5, MMP-1, and MMP-3, DuoSet ELISA development kits were used (R&D Systems).

Flow cytometry. Cells were detached using Accutase (PAA Laboratories) and washed with 1% FCS in PBS. Two microliters of mouse anti-human TLR-2 antibodies (eBioscience) or mouse IgG2aκ was added to 1 × 10^5 cells and incubated for 30 minutes at 4°C. After washing, cells were treated with 1 μl fluorescein isothiocyanate (FITC)–labeled goat anti-mouse IgG (Jackson ImmunoResearch) for 30 minutes at 4°C. Cells were washed and resuspended in 1% FCS in PBS and analyzed on a FACSCalibur flow cytometer. Data were processed using CellQuest software (BD Biosciences).

NOD-1 protein was detected by intracellular staining using a BD Cytofix/Cytoperm kit (BD PharMingen). Perme-

abilized cells were incubated for 30 minutes at 4°C with 1 μg/ml of rabbit anti-human NOD-1 antiserum or goat anti-rabbit IgG as isotype control. Cells were washed with BD Perm/Wash solution and subsequently incubated for 30 minutes at 4°C with 0.5 μg/ml of FITC-labeled goat anti-rabbit IgG (BD PharMingen). After 2 more washing steps with BD Perm/Wash solution, cells were resuspended in 1% FCS in PBS and analyzed on a FACSCalibur flow cytometer. Data were processed using CellQuest software. To show specificity of the binding of NOD-1 antibodies, antibody-blocking experiments were performed, using the same methods as described for immunohistochemistry. The blocking peptide blocked >90% of NOD-1 staining.

Western blotting. Whole cell lysates were dissolved in sample buffer (50 m*M* Tris HCl buffer [pH 6.8], 0.4% sodium dodecyl sulfate [SDS], 10% glycerol, 1.5% β-mercaptoethanol, and 0.001% bromphenol blue) and boiled at 95°C for 3 minutes. Proteins were separated in an SDS–polyacrylamide gel and transferred to nitrocellulose membranes. The membranes were blocked with 5% nonfat dry milk for 1 hour at room temperature, and then incubated overnight at 4°C with rabbit anti-human phosphorylated IL-1 receptor–associated kinase 1 (IRAK-1) antibodies (Thr^{209}; Abcam), mouse anti-human NOD-2 antibodies (clone 2D; Santa Cruz Biotechnology), mouse anti-human tubulin antibodies (Sigma-Aldrich), or mouse anti-human β-actin antibodies (Sigma-Aldrich). The membranes were washed and then incubated for 45 minutes with the respective HRP-conjugated secondary antibodies. After washing, antigen–antibody complexes were detected with an enhanced chemiluminescence Western blotting kit (GE Healthcare). Protein levels were analyzed using a Bio-Rad calibrated densitometer.

Statistical analysis. Values are presented as the mean ± SEM. Mann-Whitney U tests or Wilcoxon's signed rank tests (for paired samples) were applied to compare 2 groups. Friedman's nonparametric test followed by Dunn's test for multiple comparisons were used for comparisons of more than 2 groups, and synergistic interaction was calculated by two-way analysis of variance with replication. *P* values less than 0.05 were considered significant.

RESULTS

Expression of NOD-1 protein in RA and OA synovial tissue. We analyzed the expression of NOD-1 by immunohistochemistry in synovial tissue samples from patients with RA (n = 9) and patients with OA (n = 6), and found NOD-1 to be strongly expressed in RA synovial tissue (Figure 1A, left). Scoring of NOD-1 protein expression showed that in RA synovial tissue, expression of NOD-1 protein was significantly increased in the lining and sublining areas, when compared to that in the lining and sublining of OA synovial tissue (Figure 1A, right). The addition of a synthetic NOD-1–blocking peptide reduced the antibody staining for NOD-1 (Figure 1A, inset), thus confirming the specificity of the staining.

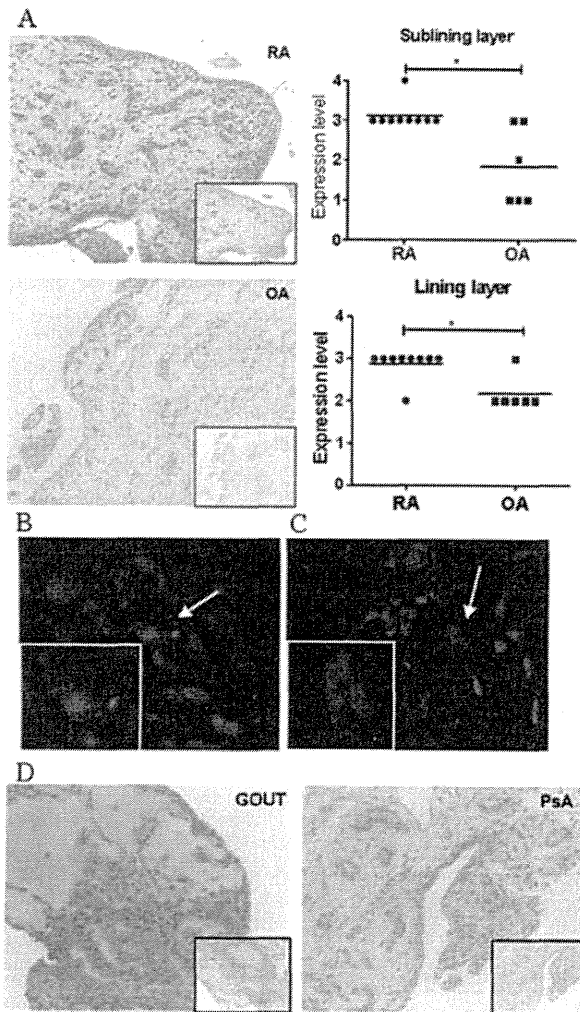To identify the specific cells in the synovium that

Figure 1. Expression of nucleotide-binding oligomerization domain–containing protein 1 (NOD-1) in rheumatoid arthritis (RA) synovial tissue. A, Left, NOD-1 expression was detected by immunostaining in synovial tissue from patients with RA and patients with osteoarthritis (OA); as negative controls, NOD-1–blocking peptide (inset, top) or isotype controls (inset, bottom) were used. Nuclei were counterstained with hematoxylin. Positive staining appears in red. Right, Staining intensities in the sublining and lining layers of RA and OA synovial tissue were scored. Bars show the mean. * = $P < 0.05$ by Mann-Whitney U test. B and C, RA synovial tissue was double stained for detection of NOD-1 (green) along with CD68 (red) as a marker for macrophages (B) or vimentin (red) as a marker for mesenchymal cells (C). Nuclei appear in blue (DAPI-stained). Arrows indicate double-stained cells. Insets show higher-magnification views (original magnification × 630). D, NOD-1 expression was assessed by immunostaining in synovial tissue from patients with gout and patients with psoriatic arthritis (PsA), with strong staining found in tissue from patients with gout. Insets show negative controls. In A–D, representative images of samples from individual patients are shown. Original magnification × 100 in A; × 400 in B and C; × 200 in D.

express NOD-1, we performed double stainings for NOD-1 and used either CD68 as a macrophage marker or vimentin as a mesenchymal cell marker. Macrophages as well as synovial fibroblasts and endothelial cells stained positive for NOD-1 (Figures 1B and C).

NOD-1 expression was also tested in patients with gout (n = 6) and patients with PsA (n = 4). While only 1 of 4 PsA synovial tissue samples expressed NOD-1, all of the gout synovial tissue samples displayed strong staining for NOD-1 (Figure 1D).

Expression and regulation of NOD-1 in different cell types. We next examined expression and regulation of NOD-1 in RASFs, OASFs, healthy control PBMCs, and healthy control HMDMs. NOD-1 was expressed by all of the cell types tested, and there was no significant difference in the basal expression of NOD-1 mRNA or protein in the different cell types (Figure 2A). Stimulation experiments showed that the levels of NOD-1 in RASFs were significantly up-regulated by the TLR-3 ligand PIC, whereas none of the other agents (the NOD-1 ligand Tri-DAP, the TLR-2 ligand Pam_3CSK_4, the TLR-4 ligand LPS, TNFα, or IL-1β) had an effect on NOD-1 transcription (Figure 2B). In contrast, in HMDMs, neither the mRNA levels nor the protein levels of NOD-1 were changed by stimulation with any of the TLR ligands tested (Figure 2C).

Expression of proinflammatory and matrix-degrading molecules after stimulation with the NOD-1 ligand. To learn more about the function of NOD-1 signaling in synovial fibroblasts, we stimulated RASFs with the NOD-1 ligand Tri-DAP and measured mRNA expression of the proinflammatory cytokine IL-6, the chemokine CCL5 (RANTES), MMPs, and the PRRs TLR-2, TLR-3, TLR-4, and NOD-2. Expression of IL-6 and CCL5 mRNA was significantly up-regulated in RASFs after 8 hours and 24 hours of stimulation with Tri-DAP (Figure 3A). The mean increase in the levels of IL-6 was 4-fold, whereas the levels of CCL5 were induced to an even greater extent, more than 20-fold, by NOD-1 activation.

In addition, the expression of MMP-1, MMP-3, and MMP-13 mRNA was significantly up-regulated by Tri-DAP (Figure 3B). The strongest effect of Tri-DAP was seen on MMP-1, which showed a mean 6.2-fold increase in mRNA levels after 8 hours and a mean 6.6-fold increase after 24 hours. MMP-3 mRNA levels were significantly increased by 5.3-fold after 24 hours, and MMP-13 mRNA levels were significantly increased by 3.6-fold after 8 hours of stimulation. MMP-9 mRNA expression was increased in some RASFs after stimulation, but the fold change was not statistically significantly different from that in unstimulated controls.

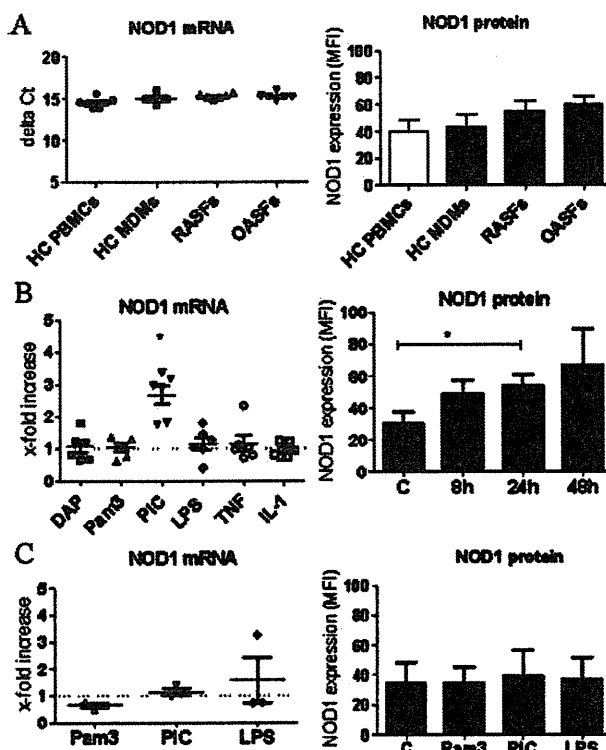With regard to the effects of NOD-1 on the

Figure 2. Expression of NOD-1 mRNA and protein in RA synovial fibroblasts (RASFs), OA synovial fibroblasts (OASFs), healthy control peripheral blood mononuclear cells (HC PBMCs), and healthy control monocyte-derived macrophages (HC MDMs). **A,** Similar expression levels of NOD-1 mRNA (n = 4–7) and protein (n = 5–6) were found in the various cell types tested. Results for mRNA are expressed as the change in threshold cycle (ΔC_t) for NOD-1 relative to 18S. **B,** After stimulation of RASFs (n = 6) with L-alanyl-γ-D-glutamyl-meso-diaminopimelic acid (Tri-DAP [DAP]), palmitoyl-3-cysteine-serine-lysine-4 (Pam_3CSK_4 [Pam3]), poly(I-C) (PIC), lipopolysaccharide (LPS), tumor necrosis factor α (TNFα), or interleukin-1β (IL-1β) for 24 hours, levels of NOD-1 mRNA significantly increased only in cells stimulated with PIC (∗ = $P < 0.05$ versus unstimulated cells, by Wilcoxon matched pairs test), and NOD-1 protein levels significantly increased at 8 hours and 24 hours after stimulation with PIC (∗ = $P < 0.05$ by Friedman's nonparametric test with Dunn's test for multiple comparisons). **C,** NOD-1 mRNA or protein expression in healthy control MDMs (n = 3) did not change after incubation with Toll-like receptor ligands or LPS for 24 hours. In **B** and **C,** changes in mRNA are assessed as the fold increase relative to that in unstimulated cells (broken line), while changes in protein are the induced change in mean fluorescence intensity (MFI) compared to unstimulated controls (C). Bars show the mean ± SEM. See Figure 1 for other definitions.

PRRs, expression of TLR-3 and TLR-4 was not induced by the NOD-1 ligand, whereas TLR-2 was up-regulated 6-fold by Tri-DAP after 8 hours of stimulation (Figure 3C). Furthermore, expression of NOD-2 was induced by NOD-1 signaling, although a significant change was seen only after 24 hours of stimulation with Tri-DAP (Figure
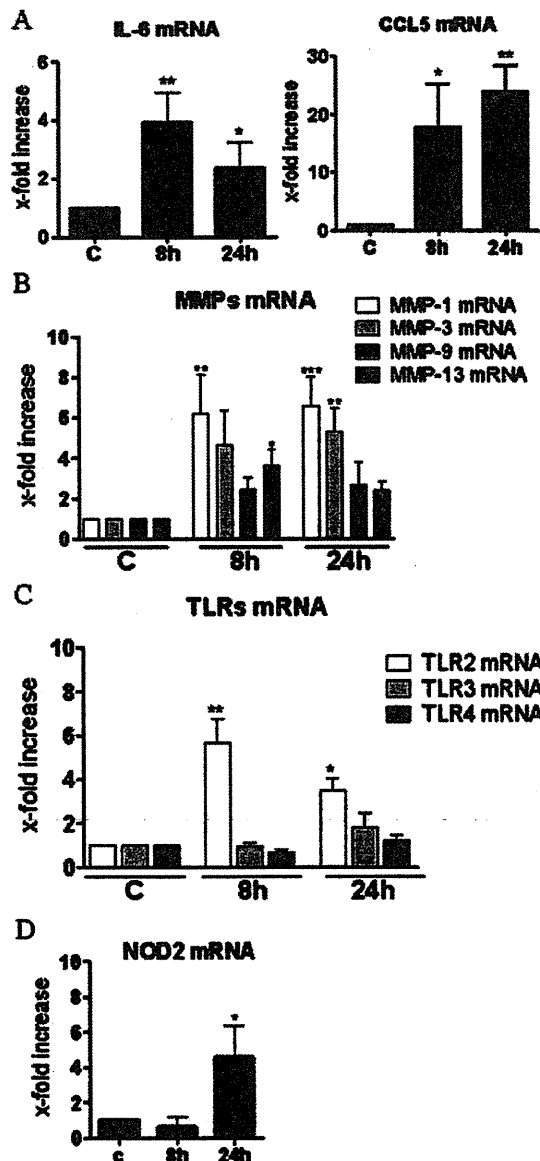

Figure 3. Induced production of proinflammatory cytokines, chemokines, matrix-degrading enzymes, and peptidoglycan-sensing pattern-recognition receptors (PRRs) following stimulation with L-alanyl-γ-D-glutamyl-meso-diaminopimelic acid (Tri-DAP) in RA synovial fibroblasts (RASFs). Incubation of RASFs (n = 6) with 10 ng/ml Tri-DAP for 8 hours and 24 hours induced a significant increase in the mRNA levels of interleukin-6 (IL-6) and CCL5 at both time points **(A)** and a significant increase in matrix metalloproteinases (MMPs) 1, 3, and 13 (but not MMP-9) at one or both time points **(B).** Among the PRRs measured at 8 or 24 hours after stimulation with Tri-DAP, only the mRNA levels of Toll-like receptor 2 (TLR-2) (n = 8) **(C)** and NOD-2 (n = 3–8) **(D)** were significantly changed. Bars show the mean ± SEM fold increase relative to unstimulated controls (C). ∗ = $P < 0.05$; ∗∗ = $P < 0.01$; ∗∗∗ = $P < 0.001$ versus unstimulated controls, by Friedman's nonparametric test with Dunn's test for multiple comparisons. See Figure 1 for other definitions.

3D). Increased expression of IL-6 (Figure 4A) and increased levels of CCL5, MMP-1, MMP-3, TLR-2, and NOD-2 (results not shown) after stimulation of RASFs with Tri-DAP were also confirmed on the protein level.

Additional time course experiments showed that stimulation of NOD-1 in RASFs induced proinflammatory mediators and MMPs in a rapid response reaction (4 hours), whereas the expression of TLR-2 and NOD-2 was up-regulated at later time points (8 hours and 24 hours, respectively) (results not shown). We also examined whether stimulation with Tri-DAP could induce TLR ligands in HMDMs (n = 3), but no change in the expression of TLR-2, TLR-3, and TLR-4 was seen after 24 hours of stimulation with Tri-DAP (results not shown).

To ensure that the proinflammatory response seen after stimulation with Tri-DAP was not due to endotoxin contamination, we added polymyxin B, which can neutralize the effect of LPS. No difference in the induction of IL-6 was seen between Tri-DAP–stimulated cells and Tri-DAP plus polymyxin B–stimulated cells (Figure 4A), confirming that the preparation of Tri-DAP was endotoxin-free.

For further confirmation that the measured effects after stimulation with Tri-DAP were solely mediated by the NOD-1 receptor, we silenced expression of NOD-1 with siRNA (Figure 4B). Knockdown of the receptor did indeed abolish the stimulatory effect of Tri-DAP in RASFs (Figure 4C).

Synergistic activity of NOD-1 with TLR-2 and TLR-4 in RASFs, and promotion of TLR-2 and IL-1 signaling. Previously, it was reported that NOD-1 can synergize with TLR-2 and TLR-4 in the production of IL-6 and IL-1β in human monocytes, dendritic cells, and PBMCs (9,14). To elucidate a possible cross-talk between NOD-1 and the TLR pathways in RASFs, co-stimulation experiments with Tri-DAP and the TLR-2 ligand Pam$_3$CSK$_4$, the TLR-3 ligand PIC, and the TLR-4 ligand LPS were performed. Similar to previously reported results in immune cells, a synergistic effect of simultaneous stimulation of NOD-1 with TLR-2 and TLR-4, but not with TLR-3, was found in RASFs (Figure 5A).

Since observations in mouse studies have suggested a modulating effect of NOD-1 on the TLR-2/NOD-2 signaling pathways (18), we tested whether knockdown of NOD-1 would have any influence on the production of IL-6 after TLR stimulation. Whereas the absence of NOD-1 in RASFs did not alter the response to TLR-3 or TLR-4 activation, IL-6 levels were 24% lower after TLR-2 stimulation when NOD-1 was knocked down, suggesting that NOD-1 has a promoting
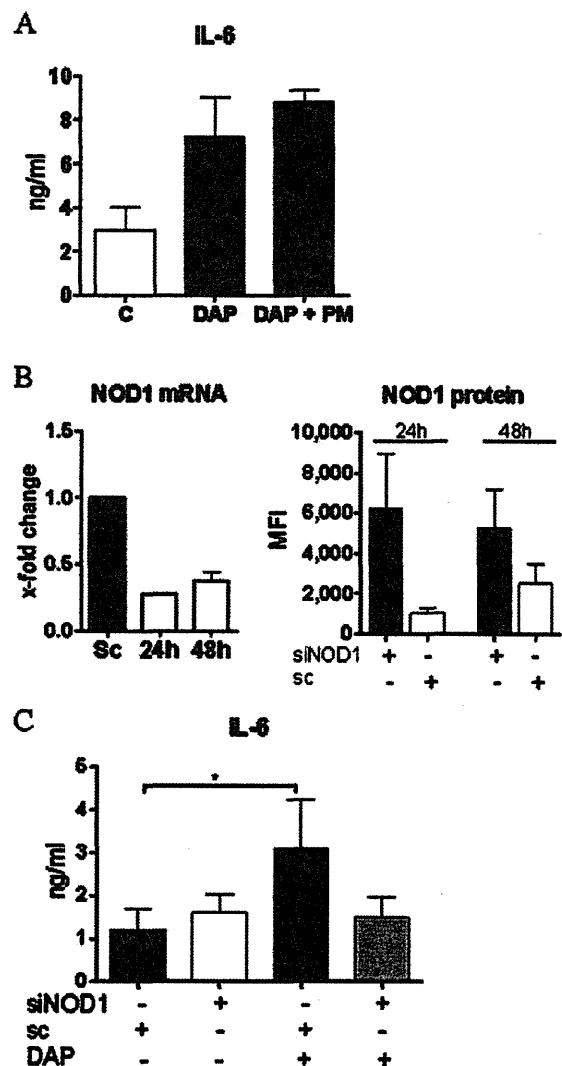

Figure 4. Specificity of L-alanyl-γ-D-glutamyl-meso-diaminopimelic acid (Tri-DAP [DAP]) in RA synovial fibroblasts (RASFs), and effects of NOD-1 silencing. A, RASFs (n = 2–6) were stimulated with Tri-DAP alone or Tri-DAP with polymyxin B (PM), or left unstimulated (control [C]), for 24 hours, and levels of interleukin-6 (IL-6) in the cell supernatants were measured by enzyme-linked immunosorbent assay. B, RASFs (n = 3–4) were transfected with scrambled control (Sc) small interfering RNA (siRNA) or NOD-1–targeting siRNA (siNOD1), and expression levels of NOD-1 mRNA and protein were measured 24 hours and 48 hours after transfection. Results for mRNA are the fold change relative to scrambled control, while those for protein are the mean fluorescence intensity (MFI) with or without gene silencing. C, Twenty-four hours after transfection of RASFs (n = 6) with NOD-1 siRNA or scrambled control siRNA, cells were stimulated with Tri-DAP for 24 hours, and levels of IL-6 were measured in the supernatants. ∗ = $P < 0.05$ by Friedman's nonparametric test with Dunn's test for multiple comparisons. Bars show the mean ± SEM. See Figure 1 for other definitions.
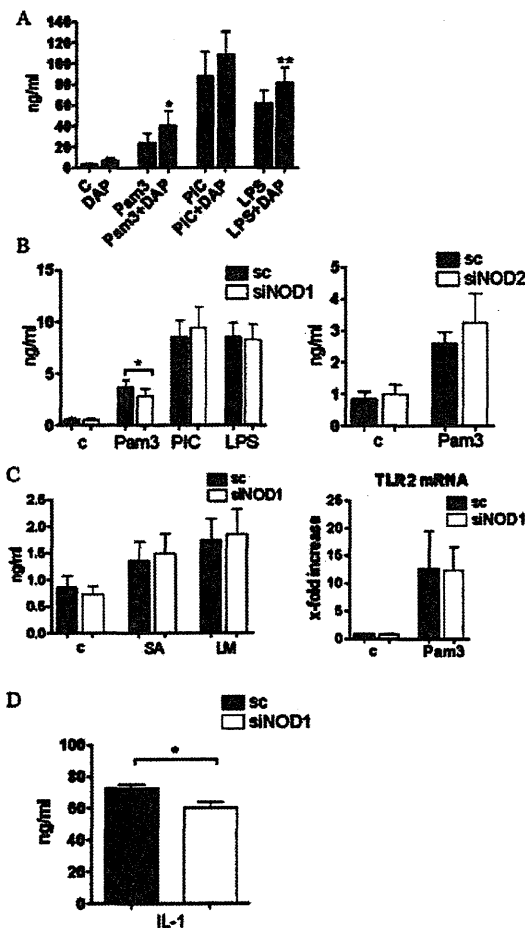
Figure 5. Down-regulation of Toll-like receptor 2 (TLR-2) and interleukin-1β (IL-1β)–induced production of IL-6 by silencing of NOD-1 in RA synovial fibroblasts (RASFs). **A,** Two-way analysis of variance showed synergistic interaction of L-alanyl-γ-D-glutamyl-meso-diaminopimelic acid (Tri-DAP [DAP]) with palmitoyl-3-cysteine-serine-lysine-4 (Pam$_3$CSK$_4$ [Pam3]) and lipopolysaccharide (LPS), but not with poly(I-C) (PIC), in the induction of IL-6 production in RASFs (n = 6). **B,** Knockdown of NOD-1 with small interfering RNA (siNOD1) in RASFs (n = 6) led to significantly decreased levels of IL-6, when compared to those in scrambled control siRNA (sc)–transfected RASFs, after Pam$_3$CSK$_4$ stimulation (left). Knockdown of NOD-2 did not induce any change in the IL-6 levels in RASFs (n = 4) after stimulation with Pam$_3$CSK$_4$ (right). **C,** Stimulation with heat-inactivated *Staphylococcus aureus* (SA) or *Listeria monocytogenes* (LM) resulted in similar levels of IL-6 in NOD-1 siRNA–transfected cells and control siRNA–transfected cells (each n = 6) (left). After stimulation with Pam$_3$CSK$_4$, TLR-2 mRNA levels were increased in both NOD-1 siRNA– and control siRNA–transfected RASFs (each n = 3) (right). **D,** IL-6 levels were significantly lower in siNOD-1–transfected cells compared with control siRNA–transfected cells (each n = 6) after stimulation with IL-1β. $*$ = P < 0.05; $**$ = P < 0.01 versus control, by Wilcoxon's matched pairs test. In **A–C,** unstimulated cells were used as treatment controls (C). Bars show the mean ± SEM. See Figure 1 for other definitions.

role in TLR-2 signaling (Figure 5B, left). No such effect was seen when NOD-2 was knocked down, as shown by the similar levels of IL-6 after TLR-2 stimulation in control siRNA–transfected cells and siNOD-2–transfected cells (Figure 5B, right).

We then tested whether the modulating effect of NOD-1 would still occur if the TLR-2 pathways were not selectively activated, and whether it must act in combination with other PRRs. The cell wall of *Staphylococcus aureus* contains TLR-2–activating peptidoglycans as well as NOD-2–activating muramyl dipeptides (MDPs). The cell wall of *Listeria monocytogenes* contains, in addition to these molecules, DAP, and therefore stimulates the TLR-2, NOD-2, and NOD-1 pathways. Our experiments with these bacterial agents showed that the double and triple activation of PRRs overruled the modulating effect of NOD-1 seen with specific TLR-2 stimulation alone, and no difference in the production of IL-6 was observed between NOD-1–silenced and control siRNA–transfected RASFs (Figure 5C, left).
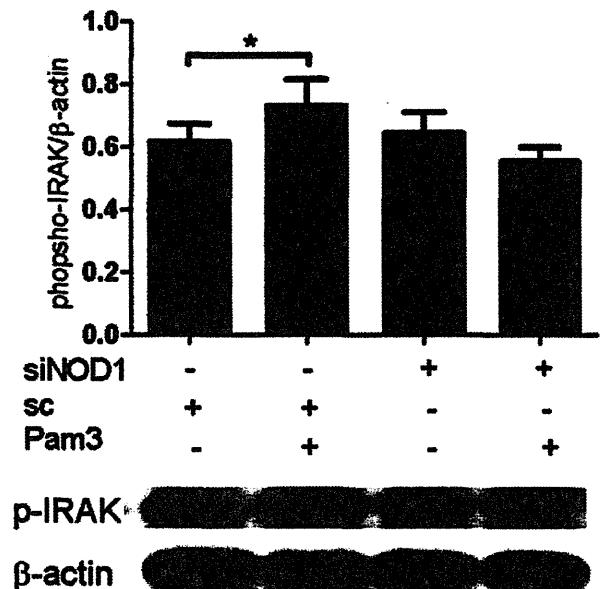

Figure 6. Influence of NOD-1 on interleukin-1 receptor–associated kinase 1 (IRAK-1) phosphorylation in RA synovial fibroblasts (RASFs). After stimulation of RASFs with palmitoyl-3-cysteine-serine-lysine-4 (Pam$_3$CSK$_4$ [Pam3]) for 20 minutes, the phosphorylation of IRAK-1, expressed as the ratio of phospho–IRAK-1 to β-actin, significantly increased in scrambled control (sc) small interfering RNA (siRNA)–transfected RASFs, but not in NOD-1 siRNA–transfected cells (top). Western blots of IRAK-1 phosphorylation in RASFs from each group are also shown, with β-actin used as a positive control (bottom). Bars show the mean ± SEM of 15 samples per group. $*$ = P < 0.01 by Wilcoxon's matched pairs test. See Figure 1 for other definitions.

Since this specific effect of NOD-1 silencing on TLR-2 signaling could be due to the down-regulation of TLR-2 itself as a result of the knockdown of NOD-1, we measured TLR-2 transcripts after the silencing of NOD-1. As described above, the levels of TLR-2 were strongly increased after incubation of the RASFs with the TLR-2 ligand. Silencing of NOD-1 had no effect on the TLR-2 levels in either unstimulated or stimulated cells (Figure 5C, right).

Among the 3 TLRs analyzed, TLR-2 is the only one that exclusively signals via the adaptor protein myeloid differentiation factor 88 (MyD88). Therefore, we hypothesized that NOD-1 might influence the MyD88 signaling pathway. If this were the case, then NOD-1 knockdown should diminish IL-1 signaling, since MydD88 is also recruited by the IL-1 receptor after ligand binding. Stimulation of NOD-1–knockdown cells with IL-1β led to an 18% reduction in the levels of IL-6 when compared to that in IL-1β–stimulated control siRNA–transfected cells (Figure 5D), corroborating a modulating role of NOD-1 in the MyD88 pathway.

Activation of MyD88 leads to phosphorylation of IRAK-1. Accordingly, we found that stimulation of RASFs with Pam$_3$CSK$_4$ for 20 minutes increased the phosphorylation of IRAK-1 (Figure 6). Knockdown of NOD-1, however, prevented the phosphorylation of IRAK-1 after stimulation with Pam$_3$CSK$_4$.

DISCUSSION

In the present study, we have shown that NOD-1 is strongly expressed in RA synovium, and that its expression can be induced in RASFs by stimulation of TLR-3. NOD-1 stimulation of RASFs led to a rapid increase in the production of proinflammatory and matrix-degrading mediators, followed by up-regulation of the expression of TLR-2 and NOD-2, and this activity of NOD-1 synergized with the stimulatory effects of TLR-2 and TLR-4 in the production of IL-6. Furthermore, knockdown of NOD-1 diminished the production of IL-6 after stimulation with Pam$_3$CSK$_4$ and IL-1β, and blocked the phosphorylation of IRAK-1.

As our results show, NOD-1 expression was increased equally in synovial fibroblasts, macrophages, and PBMCs. Furthermore, TLR-3 stimulation further increased the expression of NOD-1 in RASFs. The high levels of NOD-1 in RA synovial tissue, compared to OA synovial tissue, can therefore be attributed, most probably, to the influx of immune cells in the synovium, in conjunction with the higher NOD-1 expression in RASFs caused by the activation of TLR-3. It has been

shown that endogenous double-stranded RNA from necrotic cells can activate RASFs via TLR-3, which might be the mechanism by which expression of NOD-1 is increased in RASFs in vivo (5). The high expression of NOD-1 observed in the synovial tissue of patients with gout indicates that NOD-1 may play a pathophysiologic role in this disease as well. Similar to the NLRP3 inflammasome, which is well known to play an important role in gout, NOD-1 has been shown to bind to caspase 1 and promote IL-1 secretion (19).

Stimulation of NOD-1 led to the production of a wide range of proinflammatory mediators and MMPs in RASFs. In addition, there was a synergistic effect on the production of IL-6 in RASFs following simultaneous stimulation of NOD-1 and the TLRs. Surprisingly, HMDMs reacted to a much lower extent to stimulation with Tri-DAP than did synovial fibroblasts. Taken together, these findings highlight the important role of synovial fibroblasts as cells of the innate immune system that rapidly integrate and elicit an innate immune response. Of note, stimulation of NOD-1 selectively induced the increased expression of other peptidoglycan-sensing PRRs, namely, TLR-2 and NOD-2, but not TLR-3 and TLR-4. This indicates that there may be a directed chain reaction in the mechanisms of proper immune defense, rather than a general increase in PRRs after sensing of invading pathogens.

Exogenous ligands for PRRs, such as the NOD-2 ligand MDP, or bacterial peptidoglycans have been identified in the joints of patients with RA (18,20). Moreover, the list of endogenous ligands for PRRs continues to expand, and it has become clear that, in addition to their role in immune defense, PRRs are important sensors of tissue damage. No endogenous ligands for the NLRs NOD-1 and NOD-2 have been found up to now. In addition, it should be noted that direct interactions of NOD-1 and NOD-2 with their respective ligands have also not as yet been demonstrated. Therefore, the possibility that these NLRs respond to their ligands via an indirect mechanism cannot be excluded.

The results presented herein suggest that the presence of NOD-1 is essential for the phosphorylation of IRAK-1 in RASFs after recruitment in response to MyD88. This is particularly interesting since NLRP12, a member of the pyrin domain–containing NLR subfamily, has been shown to bind IRAK-1 and to block its phosphorylation (21). In general, accumulating evidence indicates that NLRs tend to associate with other proteins to form large complexes, and that the composition

of these complexes will determine the biologic function of the various NLRs (22).

In summary, the results of the present study demonstrate that the expression of NOD-1 is increased in the synovial tissue of RA patients, and that RASFs show a strong proinflammatory response after stimulation of NOD-1 with its ligand, Tri-DAP. Moreover, down-regulation of NOD-1 leads to reduced levels of IL-6 in RASFs after stimulation with TLR-2 or IL-1β, and will result in blocked phosphorylation of IRAK-1. Thus, our findings indicate that NOD-1, either alone or in interactions with other inflammatory mediators, plays an important role in the chronic and destructive joint inflammation in RA.

ACKNOWLEDGMENTS

AUTHOR CONTRIBUTIONS

All authors were involved in drafting the article or revising it critically for important intellectual content, and all authors approved the final version to be published. Dr. Ospelt had full access to all of the data in the study and takes responsibility for the integrity of the data and the accuracy of the data analysis.
Study conception and design. Yokota, R. E. Gay, S. Gay, Ospelt.
Acquisition of data. Yokota, Miyazaki, Kolling, Fearon, Suzuki, Ospelt.
Analysis and interpretation of data. Yokota, Hemmatazad, R. E. Gay, Fearon, Mimura, S. Gay, Ospelt.

REFERENCES

1. Zhang X, Glogauer M, Zhu F, Kim TH, Chiu B, Inman RD. Innate immunity and arthritis: neutrophil Rac and Toll-like receptor 4 expression define outcomes in infection-triggered arthritis. Arthritis Rheum 2005;52:1297–304.

2. Deng GM, Nilsson IM, Verdrengh M, Collins LV, Tarkowski A. Intra-articularly localized bacterial DNA containing CpG motifs induces arthritis. Nat Med 1999;5:702–5.

3. Strober W, Murray PJ, Kitani A, Watanabe T. Signalling pathways and molecular interactions of NOD1 and NOD2. Nat Rev Immunol 2006;6:9–20.

4. Franchi L, Warner N, Viani K, Nunez G. Function of Nod-like receptors in microbial recognition and host defense. Immunol Rev 2009;227:106–28.

5. Brentano F, Schorr O, Gay RE, Gay S, Kyburz D. RNA released from necrotic synovial fluid cells activates rheumatoid arthritis synovial fibroblasts via Toll-like receptor 3. Arthritis Rheum 2005;52:2656–65.

6. Ospelt C, Brentano F, Rengel Y, Stanczyk J, Kolling C, Tak PP, et al. Overexpression of Toll-like receptors 3 and 4 in synovial tissue from patients with early rheumatoid arthritis: Toll-like receptor expression in early and longstanding arthritis. Arthritis Rheum 2008;58:3684–92.

7. Ospelt C, Brentano F, Jungel A, Rengel Y, Kolling C, Michel BA,

8. Hisamatsu T, Suzuki M, Podolsky DK. Interferon-γ augments CARD4/NOD1 gene and protein expression through interferon regulatory factor-1 in intestinal epithelial cells. J Biol Chem 2003;278:32962–8.

9. Fritz JH, Girardin SE, Fitting C, Werts C, Mengin-Lecreulx D, Caroff M, et al. Synergistic stimulation of human monocytes and dendritic cells by Toll-like receptor 4 and NOD1- and NOD2-activating agonists. Eur J Immunol 2005;35:2459–70.

10. Chamaillard M, Hashimoto M, Horie Y, Masumoto J, Qiu S, Saab L, et al. An essential role for NOD1 in host recognition of bacterial peptidoglycan containing diaminopimelic acid. Nat Immunol 2003; 4:702–7.

11. Viala J, Chaput C, Boneca IG, Cardona A, Girardin SE, Moran AP, et al. Nod1 responds to peptidoglycan delivered by the Helicobacter pylori cag pathogenicity island. Nat Immunol 2004; 5:1166–74.

12. Welter-Stahl L, Ojcius DM, Viala J, Girardin S, Liu W, Delarbre C, et al. Stimulation of the cytosolic receptor for peptidoglycan, Nod1, by infection with Chlamydia trachomatis or Chlamydia muridarum. Cell Microbiol 2006;8:1047–57.

13. Opitz B, Puschel A, Beermann W, Hocke AC, Forster S, Schmeck B, et al. Listeria monocytogenes activated p38 MAPK and induced IL-8 secretion in a nucleotide-binding oligomerization domain 1-dependent manner in endothelial cells. J Immunol 2006;176: 484–90.

14. Van Heel DA, Ghosh S, Butler M, Hunt K, Foxwell BM, Mengin-Lecreulx D, et al. Synergistic enhancement of Toll-like receptor responses by NOD1 activation. Eur J Immunol 2005;35: 2471–6.

15. McGovern DP, Hysi P, Ahmad T, van Heel DA, Moffatt MF, Carey A, et al. Association between a complex insertion/deletion polymorphism in NOD1 (CARD4) and susceptibility to inflammatory bowel disease. Hum Mol Genet 2005;14:1245–50.

16. Hysi P, Kabesch M, Moffatt MF, Schedel M, Carr D, Zhang Y, et al. NOD1 variation, immunoglobulin E and asthma. Hum Mol Genet 2005;14:935–41.

17. Arnett FC, Edworthy SM, Bloch DA, McShane DJ, Fries JF, Cooper NS, et al. The American Rheumatism Association 1987 revised criteria for the classification of rheumatoid arthritis. Arthritis Rheum 1988;31:315–24.

18. Joosten LA, Heinhuis B, Abdollahi-Roodsaz S, Ferwerda G, Lebourhis L, Philpott DJ, et al. Differential function of the NACHT-LRR (NLR) members Nod1 and Nod2 in arthritis. Proc Natl Acad Sci U S A 2008;105:9017–22.

19. Yoo NJ, Park WS, Kim SY, Reed JC, Son SG, Lee JY, et al. Nod1, a CARD protein, enhances pro-interleukin-1β processing through the interaction with pro-caspase-1. Biochem Biophys Res Commun 2002;299:652–8.

20. Van der Heijden IM, Wilbrink B, Tchetverikov I, Schrijver IA, Schouls LM, Hazenberg MP, et al. Presence of bacterial DNA and bacterial peptidoglycans in joints of patients with rheumatoid arthritis and other arthritides. Arthritis Rheum 2000;43:593–8.

21. Williams KL, Lich JD, Duncan JA, Reed W, Rallabhandi P, Moore C, et al. The CATERPILLER protein Monarch-1 is an antagonist of Toll-like receptor-, tumor necrosis factor α-, and Mycobacterium tuberculosis-induced pro-inflammatory signals. J Biol Chem 2005;280:39914–24.

22. Ting JP, Duncan JA, Lei Y. How the noninflammasome NLRs function in the innate immune system. Science 2010;327:286–90.

et al. Expression, regulation, and signaling of the pattern-recognition receptor nucleotide-binding oligomerization domain 2 in rheumatoid arthritis synovial fibroblasts. Arthritis Rheum 2009;60: 355–63.

Transgenic Overexpression of G5PR That Is Normally Augmented in Centrocytes Impairs the Enrichment of High-Affinity Antigen-Specific B Cells, Increases Peritoneal B-1a Cells, and Induces Autoimmunity in Aged Female Mice

Masahiro Kitabatake,* Teppei Toda,* Kazuhiko Kuwahara,* Hideya Igarashi,*,[1]
Mareki Ohtsuji,†,[2] Hiromichi Tsurui,† Sachiko Hirose,† and Nobuo Sakaguchi*

To investigate signals that control B cell selection, we examined expression of G5PR, a regulatory subunit of the serine/threonine protein phosphatase 2A, which suppresses JNK phosphorylation. G5PR is upregulated in activated B cells, in Ki67-negative centrocytes at germinal centers (GCs), and in purified B220⁺Fas⁺GL7⁺ mature GC B cells following Ag immunization. G5PR rescues transformed B cells from BCR-mediated activation-induced cell death by suppression of late-phase JNK activation. In G5PR-transgenic (G5PR^Tg) mice, G5PR overexpression leads to an augmented generation of GC B cells via an increase in non-Ag–specific B cells and a consequent reduction in the proportion of Ag-specific B cells and high-affinity Ab production after immunization with nitrophenyl-conjugated chicken γ-globulin. G5PR overexpression impaired the affinity–maturation of Ag-specific B cells, presumably by diluting the numbers of high-affinity B cells. However, aged nonimmunized female G5PR^Tg mice showed an increase in the numbers of peritoneal B-1a cells and the generation of autoantibodies. G5PR overexpression did not affect the proliferation of B-1a and B-2 cells but rescued B-1a cells from activation-induced cell death in vitro. G5PR might play a pivotal role in B cell selection not only for B-2 cells but also for B-1 cells in peripheral lymphoid organs. *The Journal of Immunology*, 2012, 189: 1193–1201.

A ntigen stimulation activates naive B cells expressing Ag-specific BCRs in peripheral lymphoid organs. Activated B cells proliferate rapidly and undergo secondary Ig V region diversification with somatic hypermutation and class-switch recombination in the germinal center (GC) (1–3). B cells differentiate as proliferating centroblasts in the GC dark zone and are

*Department of Immunology, Graduate School of Life Sciences, Kumamoto University, Kumamoto 860-8556, Japan; and †Department of Pathology, Juntendo University Graduate School of Medicine, Bunkyo-ku, Tokyo 113-8341, Japan

[1]Current address: Department of Immunology, Kawasaki Medical University, Kurashiki, Okayama, Japan.

[2]Current address: Faculty of Biomedical Engineering, Toin University of Yokohama, Yokohama, Kanagawa, Japan.

Address correspondence and reprint requests to Prof. Nobuo Sakaguchi, Department of Immunology, Graduate School of Life Sciences, Kumamoto University, 1-1-1 Honjo, Chuo-ku, Kumamoto 860-8556, Japan. E-mail address: nobusaka@gpo.kumamoto-u.ac.jp

The online version of this article contains supplemental material.

Abbreviations used in this article: 7-AAD, 7-aminoactinomycin D; AICD, activation-induced cell death; bio, biotin-conjugated; αCD40, anti-CD40 mAb; FDC, follicular dendritic cell; GC, germinal center; αIgM, F(ab′)₂ fragment of anti-IgM Ab; NIP, 4-hydroxy-3-iodo-5-nitrophenylacetyl; NP, 4-hydroxy-3-nitrophenyl acetyl; NP-CGG, nitrophenyl chicken γ-globulin; NZB, New Zealand Black; PI, propidium iodide; PNA, peanut agglutinin; qRT-PCR, quantitative RT-PCR; TD-Ag, T cell-dependent Ag; TdR, thymidine deoxyribose; T_FH, follicular Th; Tg, transgene, transgenic; WT, wild-type.

found as cell cycle-arrested centrocytes in the GC light zone (4–6). GC B cells expressing high-affinity and isotype-switched BCRs are thought to be selected at the centrocyte stage by follicular dendritic cells (FDCs) presenting opsonized Ag complexes on complement receptors, thus enriching these B cells and allowing for production of high-affinity Abs against the immunizing Ag (7, 8).

During the maturation of Ag-specific B cells, centrocytes that properly react with opsonized Ag complex presumably receive survival signals from follicular Th (T_FH) cells in GCs (8). BCR stimulation induces either B cell proliferation or activation-induced cell death (AICD) through various BCR-mediated signaling pathways, including levels of intracellular Ca²⁺ mobilization and activation of MAPKs and NF-κB, which are regulated by the phosphorylation status of various signaling molecules (9–12). In BCR-mediated MAPK signaling, ERK is involved in cell proliferation (13, 14), and JNK and p38 are involved in stress response and cell death (15–17). Many studies have suggested that B cell selection is attributable to a balanced regulation of activation strengths between cell survival and apoptotic signals (18–21). We sought to identify molecules that are expressed or upregulated selectively at the centrocyte stage and regulate the phosphorylation status of BCR-mediated signal transduction molecules.

G5PR, a B″ regulatory subunit of the serine/threonine protein phosphatase 2A, is upregulated in mature B cells after BCR crosslinking via Btk signaling (22, 23). B cell-specific *g5pr* knockout mice show impaired B cell maturation, but no apparent abnormalities in BCR-mediated proliferation and related downstream signals, including tyrosine phosphorylation, Ca²⁺ influx, and MAPK or cyclin D2 activation (22). B cells in these knockout mice displayed prolonged activation of JNK and an increase in Bim phosphorylation after BCR crosslinking, resulting in depolarization of the mitochondrial membrane and an increased sen-

sitivity to BCR-mediated apoptosis. These results suggest that G5PR is necessary to maintain B cells by suppressing BCR-mediated AICD through regulation of the phosphorylation status of JNK and the proapoptotic molecule Bim.

In this study, we observed that G5PR expression is markedly augmented in the centrocytes of GCs after immunization with T cell-dependent Ag (TD-Ag) in mice. Mature GC B cells showed a marked increase in *g5pr* transcription in vivo, suggesting a positive role for G5PR in the selection of B cells in the peripheral lymphoid organs. To determine the role of G5PR upregulation in B cell survival, we generated mice expressing a *g5pr* transgene (Tg) (G5PR^{Tg}) selectively in B cells and examined the effect of G5PR overexpression on the generation of high-affinity Ag-specific B cells.

Materials and Methods

mAb against G5PR

Recombinant G5PR protein with GST (GST-G5PR) was expressed using an *Escherichia coli* expression system and purified with Glutathione Sepharose 4B (GE Healthcare, Buckinghamshire, U.K.) (24). Lewis rats were immunized with the protein together with Freund's complete or incomplete (for boosting) adjuvant. Splenocytes from immunized animals were fused with P3U1 myeloma cells to generate hybridoma cell lines. A clonal cell line secreting mAb against G5PR clone (IgG1/κ) recognized the GST-G5PR by ELISA. The specificity of the mAb was confirmed by its recognition of the G5PR protein (53 kDa) introduced in *g5pr*-cDNA–transfected WEHI-231 cells.

Mice and generation of G5PR^{Tg} mice

C57BL/6 and New Zealand Black (NZB) mice were purchased from Kyudo (Fukuoka, Japan). For the Tg vector, *g5pr* cDNA was inserted into the BamHI site of p1026x vector (kindly provided by Dr. Satoshi Takaki, National Center for Global Health and Medicine, Shinjuku-ku, Tokyo), which contains the murine *lck* proximal promoter, *immunoglobulin H-chain* gene intronic enhancer, and mutated nontranslational form of *human growth hormone* gene (25). G5PR^{Tg} mice were established on a C57BL/6 background according to standard procedures (26) and screened by PCR using primers for the *human growth hormone* gene: human growth hormone-Fw, 5'-GTGAGTTTGTGTCGAACTTGC-3'; human growth hormone-Rv, 5'-TCTATTCCGACACCCTCCAA-3'. G5PR^{Tg} mice and littermates (8–12 wk) were immunized with the TD-Ag SRBC (Nippon Biotest Lab., Tokyo, Japan) or nitrophenyl chicken γ-globulin (NP-CGG; Biosearch Technologies, Novato, CA). All mice were maintained under specific pathogen-free conditions in the Center for Animal Resources and Development, Kumamoto University. All procedures were carried out according to Center for Animal Resources and Development regulations for animal experimentation care.

Immunohistochemical analysis

Spleens were surgically excised from the mice, embedded in O.C.T. Compound (Sakura Finetech, Tokyo, Japan), and frozen immediately in liquid nitrogen. The frozen block was sliced into 6-μm-thick sections, using a Cryotome (Thermo Shandon, Cheshire, U.K.). Sections were fixed with acetone, blocked with BlockAce (DS Pharma Biomedical, Osaka, Japan), and then stained with the following reagents: anti-G5PR mAb, biotin-conjugated (bio)-peanut agglutinin (PNA) (Vector Laboratories, Burlingame, CA), anti-IgD mAb, alkaline phosphatase-conjugated anti-rat IgG (SouthernBiotech, Birmingham, AL), and HRP-conjugated streptavidin (KPL, Gaithersburg, MD). Signals were developed using a Vector Blue AP Substrate Kit (Vector Laboratories) and DAB Substrate Kit (Dako, Carpinteria, CA) and observed using a BZ-8000 microscope (Keyence, Osaka, Japan). The area of each GC was calculated as the pixel count of PNA-positive cells surrounded by IgD-positive cells, using BZ-8000 software. For immunofluorescence staining, sections were stained with the following reagents: anti-G5PR mAb, bio-PNA, FITC–anti-Ki67, bio–anti-CD35 (BD Biosciences, San Jose, CA), bio–anti-CD4, bio–anti-CD11b, bio–anti-CD11c, bio–anti-IgD, allophycocyanin-conjugated anti-CD4, allophycocyanin-conjugated streptavidin (eBioscience, San Diego, CA), allophycocyanin-conjugated anti-IgG1, allophycocyanin-conjugated anti-IgD (BioLegend, San Diego, CA), Alexa 546-conjugated anti-rat IgG, and Alexa 488-conjugated streptavidin (Invitrogen, Carlsbad, CA). The signal was observed using a FV500 confocal microscope with Fluoview software (Olympus, Tokyo,

Japan). For the Z-stacks, the digital images were serially captured every 1-μm slice. For the detection of immune complexes in the kidney, sections were fixed in 4% paraformaldehyde in PBS for 10 min, blocked with Fc block (anti-CD16/32 mAb; BD Biosciences), and stained with Alexa 488-conjugated anti-mouse IgG Ab and anti-C3 mAb.

Flow cytometric analysis and cell sorting

Cell surface staining was performed with various combinations of mAbs after blocking with anti-CD16/32 mAb (eBioscience). The reagents used were as follows: FITC–anti-CD11b (BioLegend), FITC–anti-CD3, FITC–anti-CD4, FITC–anti-B220, PE–anti-CD5, PE–anti-CD19, PE–anti-CD21, allophycocyanin-conjugated anti-B220, allophycocyanin-conjugated anti-IgM (eBioscience), FITC–anti-GL7, PE–anti-Fas, PE–anti-PD-1, PECy7–anti-Fas, bio–anti-CD43, bio–anti-CXCR5 (BD Biosciences), PE–4-hydroxy-3-iodo-5-nitrophenylacetyl (NIP; kindly provided by Dr. Toshitada Takemori, Riken Research Center for Allergy and Immunology, Yokohama City, Kanagawa, Japan), and streptavidin–PerCP-Cy5.5 (BD Biosciences). After washing, flow cytometric analysis was performed on a FACSCalibur, using CellQuest software (BD Biosciences), and data were analyzed with FlowJo software (Tree Star, Ashland, OR). Spleen B-2 cells were isolated using a mouse B cell isolation kit and an autoMACS separator (Miltenyi Biotec, Bergisch Gladbach, Germany) according to the manufacturer's protocol. Cell sorting of peritoneal B-1a (CD5$^+$B220$^+$), GC (B220$^+$Fas$^+$GL7$^+$) B cells, non-GC (B220$^+$Fas$^-$GL7$^-$) B cells, and T$_{FH}$ (CD4$^+$PD-1$^+$CXCR5$^+$) cells was performed using the JSAN Cell Sorter System (Bay Bioscience, Kobe, Japan).

Cell culture, retroviral infection, and in vitro stimulation

WEHI-231 B cells and primary B-1 and B-2 cells were cultured in RPMI 1640 medium (Invitrogen) supplemented with 10% heat-inactivated FCS (Thermo Trace, Waltham, MA), 2 mM L-glutamine, 50 μM 2-ME (Wako, Osaka, Japan), 200 U/ml penicillin G potassium, 100 μg/ml streptomycin sulfate (Meiji Seika, Tokyo, Japan), and 10 mM HEPES (Invitrogen). For retroviral infection, *g5pr* cDNA with a 3xFLAG-tag sequence at the 5'-end was inserted into the SalI site of a pFB-IRES-GFP retroviral vector (Agilent Technologies, Santa Clara, CA) and transfected into PLAT-E ecotropic retrovirus packaging cells (kindly provided by Dr. Toshio Kitamura, University of Tokyo, Tokyo, Japan). After 2 d, retrovirus was recovered from culture supernatant, combined with 8 μg/ml polybrene (Sigma-Aldrich, St. Louis, MO), and used to infect WEHI-231 cells. GFP$^+$ cells were sorted using a JSAN Cell Sorter System. For in vitro stimulation, cells were cultured at a density of 2 × 10^6 cells/ml with 10 μg/ml F (ab')$_2$ fragment of anti-IgM Ab (αIgM; ICN Biomedicals, Costa Mesa, CA) and/or 1 μg/ml anti-CD40 mAb (αCD40; purified from LB429 culture supernatant) at several time points. After 24 h stimulation, cultures were assessed for apoptotic cells by staining with Annexin V^{FITC}, 7-aminoactinomycin D (7-AAD), active caspase 3 (BD Biosciences), or propidium iodide (PI), and flow cytometric analysis was performed on a FACSCalibur. For the cell proliferation assay, 5 × 10^4 cells were stimulated with 10 μg/ml αIgM or 5 μg/ml LPS in 96-well plates for 48 h and pulsed with [^{3}H]-thymidine deoxyribose (TdR) during the last 16 h of the culture. After stimulation, cells were harvested onto glass fiber filters (Applied Biosystems), and incorporation of [^{3}H]-TdR was measured using a scintillation counter (MicroBeta 1450; Wallac, Turku, Finland).

Preparation of RNA, RT-PCR, and quantitative RT-PCR

Total RNA was purified using an RNeasy Micro Kit (Qiagen, Hilden, Germany). The cDNAs were prepared with SuperScript III (Invitrogen) and then amplified by PCR with Z-taq (Takara Bio, Ohtsu, Japan), using the primers 5'-GGTTAGCGTCGCCCAACACG-3' and 5'-GATTCCTCTCG-TAATTTCTG-3' for *g5pr* and 5'-CCTAAGGCCAACCGTGAAAAG-3' and 5'-TCTTCATGGTGCTAGGAGCCA-3' for *β-actin*. Quantitative RT-PCR (qRT-PCR) was carried out using TaqMan gene expression assays (*bim*, Mm00437796; *g5pr*, Mm01257828; *β-actin*, Mm00607939; Invitrogen) using the ABI7500 and Sequence Detection System software (Life Technologies, Grand Island, NY). The fold change in the copy number of the transcripts was calculated using the 2$^{-\Delta\Delta Ct}$ method, with *β-actin* as the internal control.

Western blot analysis

Cells were lysed with TNE buffer (1% Nonidet P-40; 150 mM NaCl; 10 mM Tris-HCl, pH 7.5; 1 mM EDTA) containing a protease inhibitor mixture (Nacalai tesque, Kyoto, Japan). The lysate was subjected to SDS-PAGE and then transferred to a nitrocellulose membrane (Protoran, GE Healthcare). The membrane was blotted with primary Abs against p-ERK, p-p38, p-Akt, p-IκBα, p-JNK, p-c-Jun (Cell Signaling Technology, Danvers, MA), Bim
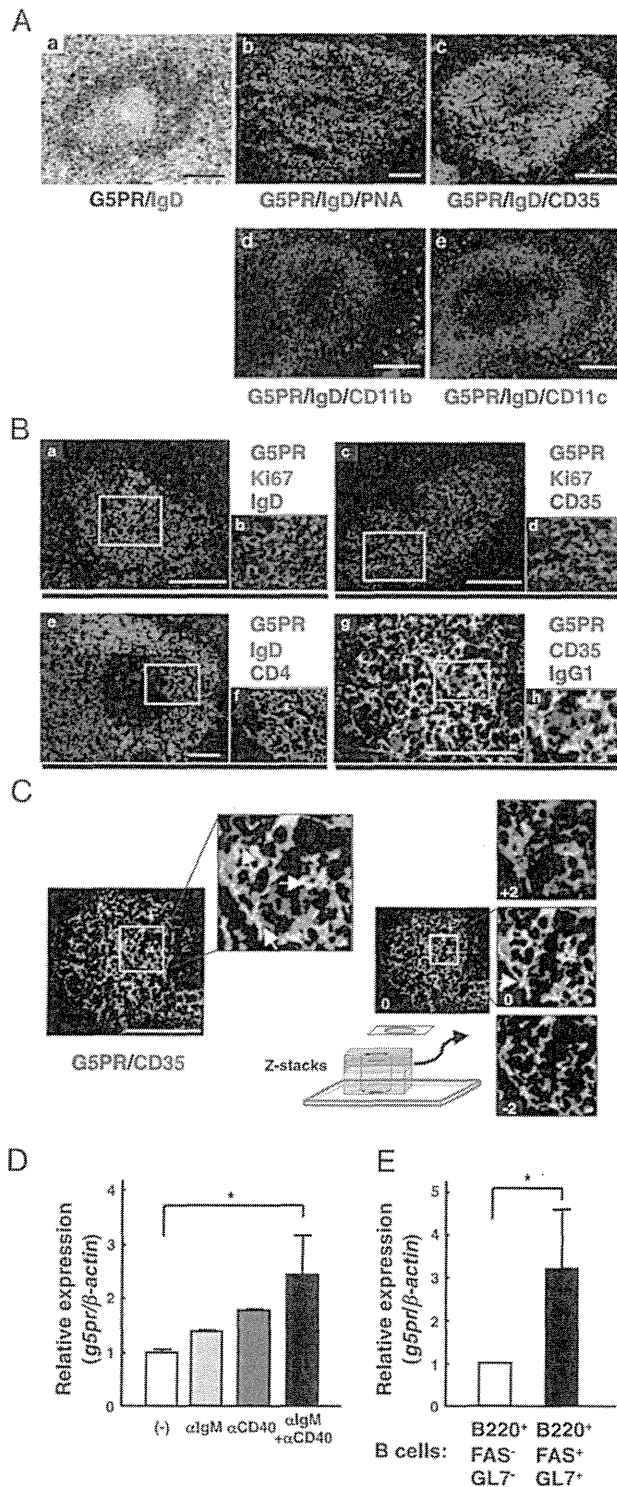
FIGURE 1. G5PR upregulation in centrocytes. (**A** and **B**) C57BL/6 mice were immunized with SRBC for 10 d, and the follicular region of their spleens was analyzed by immunohistochemistry. (A) Immunohistochemistry for G5PR/IgD (**a**) and immunofluorescent staining for G5PR/IgD/PNA (**b**), G5PR/IgD/CD35 (**c**), G5PR/IgD/CD11b (**d**), and G5PR/IgD/CD11c (**e**). (B) The sections were stained for visualization of G5PR/Ki67/IgD (**a**, **b**), G5PR/Ki67/CD35 (**c**, **d**), G5PR/IgD/CD4 (**e**, **f**), and G5PR/CD35/IgG1 (**g**, **h**). Scale bars, 100 μm. The results are representative of three independent experiments. (**C**) The GC sections were stained with G5PR/CD35 and are shown as Z-stack images. (**D** and **E**) Measurement of g5pr transcripts by qRT-PCR. (D) Spleen B cells were stimulated with αIgM and/or αCD40 for 48 h in vitro. The amount of g5pr transcript was

(Stressgen Biotechnologies, Victoria, BC, Canada), β-actin (Sigma-Aldrich), FLAG (Agilent Technologies), or GFP (Nacalai Tesque). After washing, the membrane was blotted with HRP-conjugated anti-mouse, anti-rat, or anti-rabbit Ab (Invitrogen), and then proteins were visualized with ECL Reagent (Millipore, Billerica, MA) using Versadoc (BioRad, Hercules, CA).

ELISA

Anti-dsDNA Abs were detected by ELISA, as described previously (27). Briefly, serially diluted sera were incubated for 1 h at room temperature in 96-well plates coated with 250 ng dsDNA (Sigma-Aldrich). After washing, the captured Ab was reacted with alkaline phosphatase–anti-mouse-IgM (μ-chain specific; Sigma-Aldrich) in combination with p-nitrophenyl peroxidase substrate (Sigma-Aldrich). The Ag–Ab reaction was measured by the absorbance at 405 nm, using an ImmunoMini NJ-2300 plate reader (System Instruments, Tokyo, Japan). An arbitrary unit for anti-dsDNA titer was defined by the serial dilution of pooled sera from NZB mice (10 mice) >40 wk of age.

Affinity measurement of anti–4-hydroxy-3-nitrophenyl acetyl Abs

To detect 4-hydroxy-3-nitrophenyl acetyl (NP)-specific Abs, serially diluted sera were incubated in 96-well plates coated with 10 μg/ml NP_2-BSA or NP_{25}-BSA (Bioresearch). After washing, the captured Ab was incubated with alkaline phosphatase–anti-mouse-IgG (γ-chain specific; Sigma-Aldrich) in combination with p-nitrophenyl peroxidase substrate. The Ag–Ab reaction was calculated by measuring the absorbance at 405 nm, using an ImmunoMini NJ-2300 plate reader. Relative anti-NP Ab titers were defined by the serial dilution of sera from wild-type (WT) mice. The relative affinity of the anti-NP Ab was estimated by calculating the ratio of the ELISA measurements as anti-NP_2/anti-NP_{25}.

Immunofluorescence analysis for anti-nuclear Abs

Anti-nuclear Ab was detected using an ANA-HEp-2 Immunofluorescence Kit (ORGENTEC Diagnostika, Mainz, Germany), according to the manufacturer's protocol. Briefly, 80-fold diluted sera were reacted with HEp2 cells on the slide for 30 min at room temperature. After washing with PBS, Ag–Ab complex was detected with Alexa 488-conjugated anti-mouse IgG Ab. The signal was observed using a fluorescence microscope BZ-8000.

Statistical analysis

Data are presented as the mean ± SD. Statistical analysis was performed by Student t test. A p value < 0.05 was considered statistically significant.

Results

Upregulation of G5PR expression in GC B cells

We prepared a mAb against G5PR for immunohistochemical staining and analyzed the location of $G5PR^+$ cells in the spleen after immunization with SRBC. We observed $G5PR^+$ cells in the follicular region, which contained PNA^+ GC B cells surrounded by IgD^+ B cells (Fig. 1Aa, Fig. 1Ab), and in the GC region, which contained a $CD35^+$ FDC network (Fig. 1Ac), but not in the splenic white pulp area containing $CD11b^+$ macrophages and $CD11c^+$ dendritic cells (Fig. 1Ad, Fig. 1Ae). $G5PR^+$ B cells could be distinguished from IgD^+ B cells and $Ki67^+$ proliferating centroblasts in GCs (Fig. 1Ba, Fig. 1Bb) but could be seen interacting with $CD35^+$ FDCs (Fig. 1Bc, Fig. 1Bd). $G5PR^+$ cells seem to attach to the $CD4^+$ T cells in the follicular region (Fig. 1Be and Fig. 1Bf). Some $G5PR^+$ cells coexpressed IgG1 in GCs (Fig. 1Bg and Fig. 1Bh) and interacted with FDCs, as shown in the tricolor image (white). To confirm the interaction further, two-color imaging of the interactions between $G5PR^+$ cells and FDCs (shown by a merged yellow signal) was demonstrated clearly by Z-stack analysis (Fig. 1C).

compared with that of unstimulated B cells. (E) C57BL/6 mice were immunized with SRBC for 14 d. $B220^+Fas^+GL7^+$ GC B cells were sorted as described in Supplemental Fig. 1. The amount of g5pr transcript was compared with that of $B220^+Fas^-GL7^-$ B cells. Results are shown as the mean ± SD of three independent experiments. *p < 0.05.

We next examined G5PR upregulation in splenic B cells cultured in vitro by qRT-PCR. B cells stimulated with αIgM showed a modest increase in *g5pr* transcription (Fig. 1D), which was further increased by costimulation with αIgM and anti-CD40 mAb. B220[+]Fas[+]GL7^{+} mature GC B cells purified from SRBC-immunized mice (Supplemental Fig. 1) showed significantly higher *g5pr* transcription, compared with B220[+]Fas[−]GL7^{−} B cells (Fig. 1E). Thus, G5PR is expressed at a high level in centrocytes that have undergone isotype maturation and are closely interacting with FDCs in GCs.

Effect of G5PR upregulation upon BCR-mediated AICD in a B cell line

To assess the effect of G5PR upregulation on B cell survival, we transfected WEHI-231 B cells with a FLAG-tagged G5PR vector coexpressing enhanced GFP using a bicistronic retroviral expression system and compared between cells transduced with this vector and enhanced GFP-only vector (Fig. 2A). The control and G5PR transfectants were examined for sensitivity to BCR-mediated AICD. Increased expression of G5PR significantly enhanced cell survival, as analyzed by PI staining (Fig. 2B).

Effect of G5PR upregulation on BCR-mediated signal transduction

The activation of various BCR-mediated signal transduction molecules was examined in G5PR transfectants. Phosphorylation of ERK, p38, Akt, or IκBα was not affected by G5PR expression (Fig. 2C). JNK phosphorylation was similar in control and G5PR transfectants at 5 min after stimulation, but enhanced JNK de-
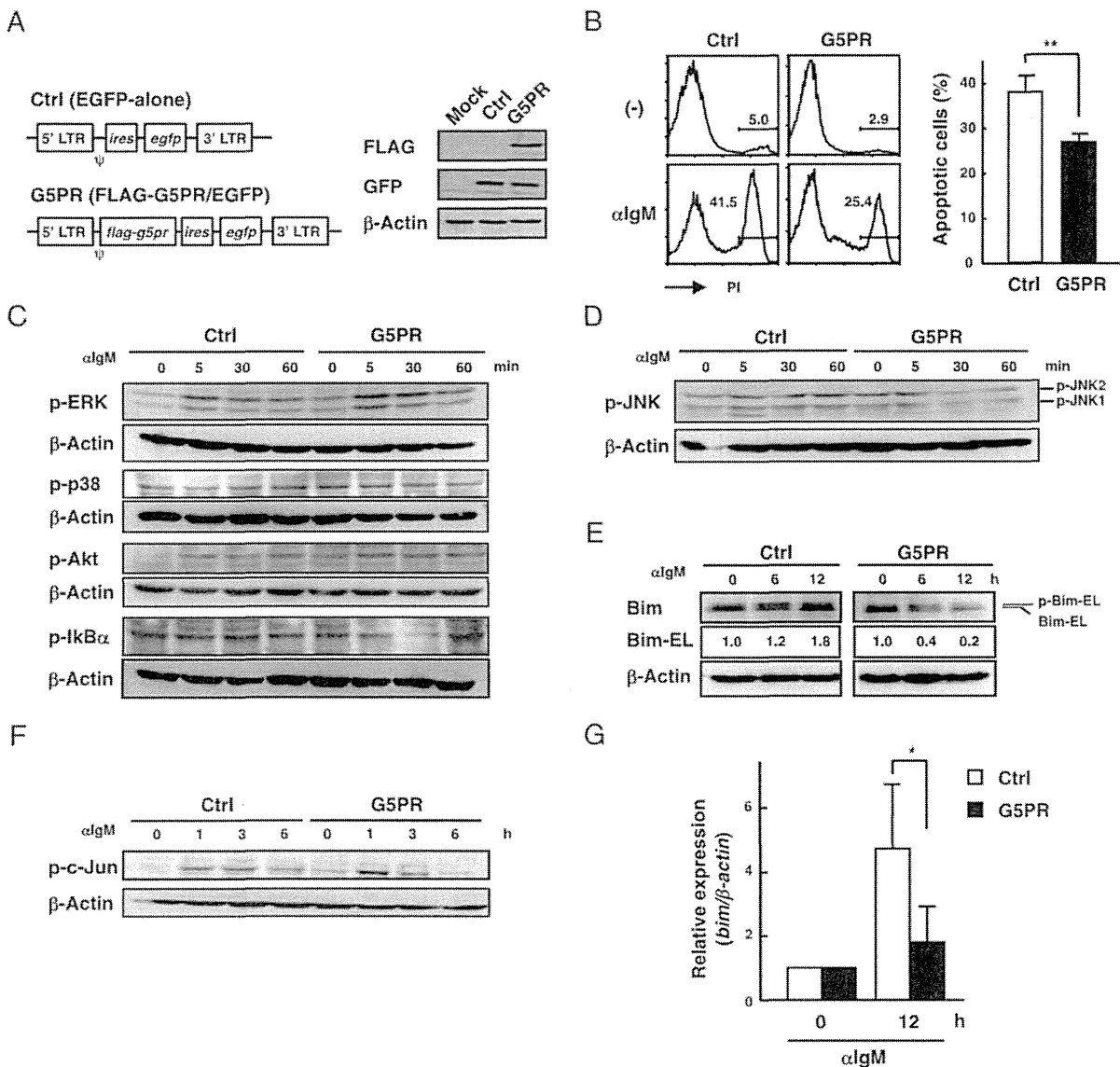

FIGURE 2. Effect of G5PR upregulation on BCR-mediated AICD and signal transduction in WEHI-231 cells. (**A**) A schematic of the *g5pr* Tg construct. WEHI-231 cells were transfected with *gfp* (Ctrl) or *flag-g5pr-ires-gfp* (G5PR) constructs using a retroviral system, and GFP^{+} cells were sorted (purity > 90%). Expression of the introduced genes was analyzed by Western blotting against FLAG and GFP. β-Actin was used for loading controls. (**B**) Cell death of G5PR transfectants by BCR crosslinking. Cells were stimulated with αIgM for 24 h, and apoptotic cells in the control or G5PR transfectants were identified by PI staining and flow cytometric analysis. Results are shown as the mean ± SD of five independent experiments. **$p < 0.01$. (**C–F**) BCR-mediated activation of signal transduction molecules. Whole-cell lysates from control or G5PR transfectants stimulated with αIgM at the indicated time were blotted using Ab against p-ERK, p-p38, p-Akt, p-IκBα (C), p-JNK (D), Bim (E), and p-c-Jun (F). β-Actin was used for loading controls. Results are representative of three independent experiments. (**G**) Expression of *bim* transcripts. Control or G5PR transfectants were stimulated with αIgM for 12 h, and *bim* transcripts were measured by qRT-PCR. Results are shown as the mean ± SD of three independent experiments. *$p < 0.05$.

phosphorylation was seen at 60 min in the G5PR transfectants (Fig. 2D). Among the Bcl-2 family molecules, the expression of antiapoptotic molecules Bcl-2 and Bcl-xL was not altered after stimulation of cells transfected with either vector (data not shown), but G5PR transfectants showed a reduced level of Bim-EL expression at 12 h after αIgM stimulation (Fig. 2E). The phosphorylation of c-Jun, a downstream molecule of JNK, was

also lower at 6 h after αIgM stimulation in G5PR transfectants (Fig. 2F). qPCR analysis showed that G5PR overexpression suppressed the augmentation of *bim* transcription caused by αIgM stimulation (Fig. 2G). Thus, although G5PR upregulation only modestly rescued B cells from rapid BCR-mediated apoptosis, it significantly altered BCR-mediated JNK-c-Jun activation, leading to altered transcription of target *bim*.

Effect of increased G5PR expression on B cells in vivo

To explore the effect of G5PR upregulation in B cells of peripheral lymphoid organs, we developed G5PR^{Tg} mice that overexpress *g5pr* transcripts in lymphoid cells under the *lck* promoter, *IgH-*
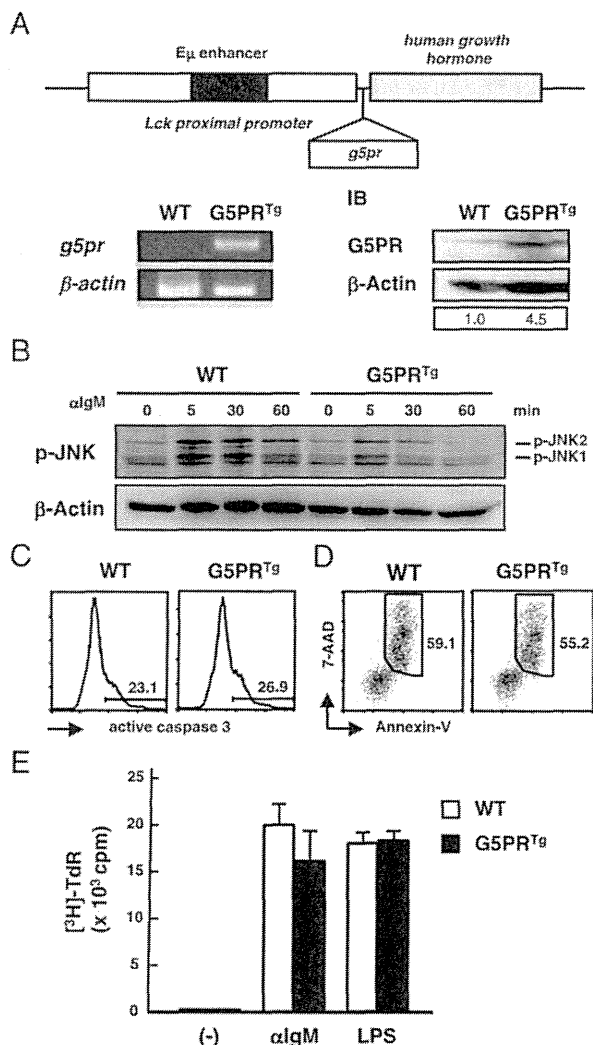

FIGURE 3. BCR-mediated apoptosis of B-2 cells in G5PR^{Tg} mice. (A) A schematic diagram of the vector construct of the Tg used to generate G5PR^{Tg} mice. Full-length *g5pr* cDNA was inserted into a p1026x vector containing an *Lck* proximal promoter and an Eμ enhancer. Spleen B cells were purified from WT and G5PR^{Tg} mice. Tg expression was analyzed by RT-PCR for *g5pr* transcripts and by Western blotting for G5PR protein. Results are representative of two independent experiments. (B) Activation of JNK in splenic B cells. Splenic B cells of WT and G5PR^{Tg} mice were stimulated with αIgM for the indicated times. Whole-cell lysates were subjected to SDS-PAGE and analyzed by immunoblotting with anti–p-JNK Ab. Anti–β-actin mAb was used as the internal control. Results are representative of two independent experiments. (C and D) BCR-mediated AICD of splenic B cells. Splenic B cells of female WT or G5PR^{Tg} mice (12 wk after birth) were stimulated with αIgM for 24 h. Apoptotic cells were analyzed by induction of active caspase 3 (C) or Annexin V^{FITC} and 7-AAD (D) staining by flow cytometry. (E) Proliferation of splenic B cells. Splenic B cells from female WT or G5PR^{Tg} mice (12 wk after birth) were stimulated with αIgM or LPS for 48 h. Incorporation of [^{3}H]-TdR was measured using a scintillation counter. Results are representative of three independent experiments.
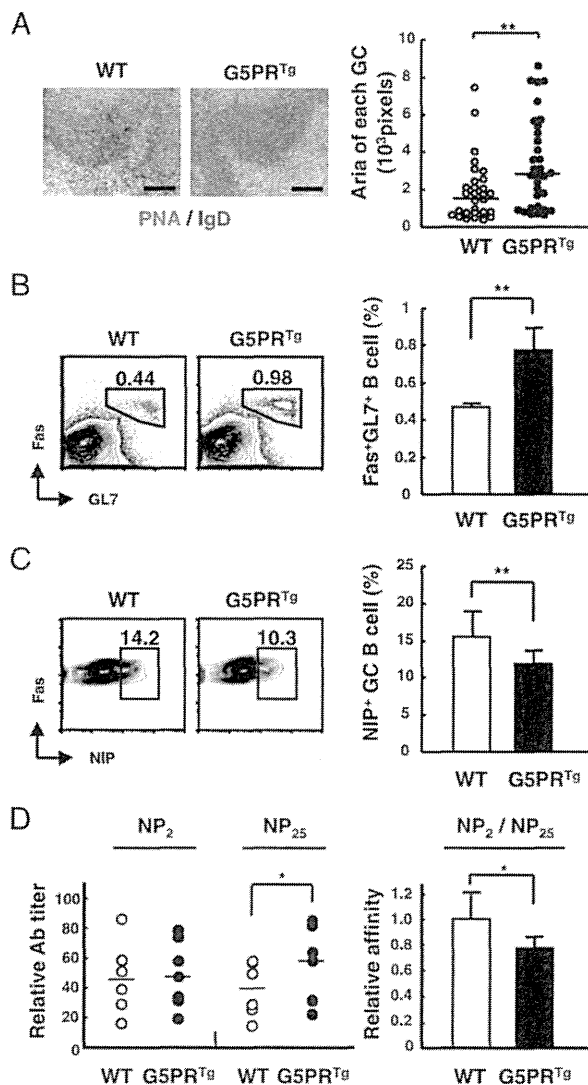

FIGURE 4. GC formation and B cell selection in G5PR^{Tg} mice. (A) Generation of GC B cells after immunization. The G5PR^{Tg} mice and littermates (*n* = 4) were immunized with SRBC for 10 d, and the spleen sections were analyzed by immunohistochemistry with PNA and IgD staining. Left panel shows the size of each GC by measuring the area of PNA staining. Scale bars, 100 μm. Result is shown as the median ± SD. (B–D) The G5PR^{Tg} mice (*n* = 7) and littermates (*n* = 6) were immunized with NP-CGG in alum for 14 d, and spleen GC B cells were characterized by flow cytometry. The frequencies of B220$^+$Fas$^+$GL7$^+$ GC B cells (B) and NIP$^+$ GC B cells (C) were compared. NP-specific IgG titers were measured by ELISA plates coated with NP$_2$-BSA (high-affinity) or NP$_{25}$-BSA (low-affinity), and the relative affinity for NP-specific IgG was calculated by NP$_2$/NP$_{25}$. Results are shown as the mean ± SD. *p < 0.05, **p < 0.01.